Development of a Portable Scratch Test Device for Probing Strength, Ductility and Structural Distress in Metal Materials

by

Steven D. Palkovic

B.S., Civil Engineering

Northeastern University, 2012

SUBMITTED TO THE DEPARTMENT OF CIVIL AND ENVIRONMENTAL ENGINEERING IN PARTIAL FULFILLMENT OF THE REQUIREMENTS FOR THE DEGREE OF

MASTER OF SCIENCE IN CIVIL ENGINEERING AT THE MASSACHUSETTS INSTITUTE OF TECHNOLOGY

JUNE 2014

Signature redacted

Author . . . . . .

Department of Civil and Environmental Engineering

May 15, 2014

Signature redacted

Certified by. . . . . .

Thomas W. Eagar

Professor of Materials Science Engineering & Engineering Systems

Thesis Supervisor

Signature redacted

Read by. . . . . .

Oral Buyukozturk

Professor of Civil and Environmental Engineering

Thesis Reader

Signature redacted

Accepted by . . . . . .

Heidi M. Nepf

Chair, Departmental Committee for Graduate Students

Development of a Portable Scratch Test Device for Probing Strength, Ductility and Structural Distress in Metal Materials

by

Steven D. Palkovic

Submitted to the Department of Civil and Environmental Engineering
on May 15, 2014 in partial fulfillment of the requirements for the degree of
Master of Science in Civil and Environmental Engineering

Abstract

Practicing civil, mechanical, aerospace, petroleum and structural engineers are often faced with the complexity of evaluating the quality and integrity of new or existing structures. Recent academic research has demonstrated that instrumented scratch testing is a viable alternative for determining the strength and ductility of metals without the use of destructive methods involving the extraction of tensile testing specimens. Although the scientific basis for scratch testing is well established, there is a necessity for a simple and robust implementation that avoids the complexities of current methods which require expensive laboratory equipment and sophisticated data processing. A detailed description of the instrumented scratch testing method for characterizing ductile metals is provided, as well as comparisons with existing alternatives. An innovative scratch testing method is proposed and validated to perform a displacement controlled scratch experiment. A portable scratch testing device is designed and developed to utilize the displacement control technique along with specific instrumentation to allow for the continuous measurement of material properties along the length of a scratch during the experiment. The scratch testing device and method are implemented in a scratch experiment on a welded connection. For the first time, a simple experimental procedure allows for the measurement of changes in mechanical properties through the weld, from the base metal, heat-affected zone (HAZ) and filler weld metal. This novel application highlights the unique ability of the scratch testing method to monitor the evolution of localized mechanical properties in areas of interest to practicing engineers. Recommendations for future iterations of the portable scratch tester are provided.

Thesis Supervisor: Thomas W. Eagar

Title: Professor of Materials Science Engineering & Engineering Systems

Thesis Reader: Oral Buyukozturk

Title: Professor of Civil and Environmental Engineering

Table of contents

List of Figures and Captions

List of Tables and Captions

Introduction

Material characterization is important in engineering to be able to predict the capacity of materials and structures. The traditional method for determining mechanical properties is to extract a sample from the assembled structure or final product and perform a tensile test to failure. This is not appropriate for non-destructive testing (NDT), which entails the evaluation of a material's capacity without jeopardizing function. For these instances, alternative testing methods utilizing contact mechanics are more appropriate.

In contact mechanics, the interaction between contacting bodies generates significant pressure which often leads to localized plasticity, while the stresses in the bulk material remains unchanged. The physical conditions of contact, including size of asperities, lubrication, relative velocities, and material properties, have significant influences on the response. These observations have led to the use of contact mechanics to simulate wear and tribological responses, the plastic behavior of ductile materials, and the fracture toughness for relatively brittle materials. Two common methods which utilize contact mechanics to evaluate mechanical properties are normal indentation and scratch hardness testing.

Normal indentation has been used for decades to determine a material's hardness. In normal indentation, a hard indenter is pressed into the surface of a softer material with a known load and the resulting indentation is measured. Therefore, hardness is an extrinsic property of a material which is a measure of the material's resistance to local deformation from an applied mean pressure. Indentation hardness tests can be performed on various size scales (macro, micro, and nano) to allow for Non-Destructive Examination (NDE) of materials.

Scratch testing of materials may also be used for material characterization. During scratch testing, a hard indenter is pressed into a softer material, and then ploughs through the material when a tangential force is applied parallel to the free surface. The resulting residual scar through the material is subsequently measured to determine the scratch hardness for a given applied load. Like with normal indentation, scratch testing results can be correlated to different deformation modes of a material, and can be performed on multiple size scales.

For practical applications, normal indentation and scratch testing experiments must be related to common material design properties such as the Young's Modulus, E, initial yield strength, σ_y, and plastic strain hardening exponent, n, which are frequently obtained through uniaxial tensile testing. This is readily accomplished through the use of reverse algorithms derived from

numerical methods such as Finite Element Analysis (FEA). Dao *et al.* proposed analytical equations that relate normal indentation experiments to elastic-plastic material properties [1]. Bellemare *et al.* implemented a similar procedure to derive analytical equations to extract elastic-plastic properties from instrumented scratch testing experiments [2,3,4]. Specifically, both sets of algorithms are used to determine the initial yield strength and plastic strain hardening exponent. These algorithms were well verified through experimental testing and are applicable for a wide range of engineering materials, allowing for the accurate extraction of mechanical properties through non-destructive testing.

Although reverse algorithms exist for both experimental methods, scratch testing is less prevalent in industry than normal indentation for elastic-plastic material characterization. This is because the testing apparatus, physical principles, and testing procedures for normal indentation hardness are well understood and simple to implement. Although analytical models of scratch testing have been proposed [5], a full understanding of the three dimensional stress-strain fields requires numerical tools like Finite Element Analysis. Despite its greater complexity and limited availability, scratch testing offers several advantages over normal indentation. These include an increase in the amount of plastic strain, a greater sampling volume from a single scratch experiment, and less sensitivity to experimental error [2,3,4]. In addition, materials that exhibit the same normal indentation hardness can have significantly different scratch hardness and scratch pile-up behavior [4].

Currently, modern scratch testing devices are limited to large and expensive laboratory equipment, while portable normal indentation devices are commercially available. This limitation reduces the prevalence and potential applications of scratch testing. Based on this observation, and the advantages of scratch testing when compared to normal indentation described above, a portable scratch tester would greatly benefit the engineering community.

For my thesis, I will design and construct a prototype for a scratch testing device that is suitable for attachment to a mobile support that will allow for in situ scratch experiments. The device will sustain both normal and tangential loads to plough across a material's surface and create a scratch profile using a tungsten carbide indenter. The existing technology is not appropriate for in situ testing, due to the difficulty with measuring the necessary parameters of the scratch experiment. Therefore this thesis proposes and validates an innovative technique which greatly simplifies the scratch testing method proposed by Bellemare et al., such that it can be applied to existing structures and assemblies. The scratch test is changed from a traditional load control

to displacement control, where the depth of the indenter penetrating the material is fixed, and the remaining characteristics are measured during the scratch experiment. The measurements are input into the reverse analytical functions proposed and verified by Bellemare *et al.* to extract mechanical properties. Therefore this device will provide a testing procedure which is quick and simple to implement, as well as allow for scratch measurements to be performed outside of a laboratory environment.

This thesis will focus on one potential application for the proposed device, which is the characterization of fabricated welded connections. This is due to the wide prevalence of welded connections as well as the variability in quality due to fabrication methods. Welds are used in a variety of joining applications which include buildings, bridges, pipelines, aerospace and automotive. Depending on the technique and conditions during fabrication, welded connections are susceptible to significant residual stresses, distortion, porosity, cracks and inclusions. These are especially prevalent in the heat-affected zone (HAZ) of the base metal, where the material's strength and ductility are changed due to rapid heating and solidification, thermal stresses, and changes to microstructure during the welding process.

The characterization of welded connections also highlights a unique feature of the instrumented scratch test, which is the ability to quantify the evolution of plastic strain hardening behavior through the HAZ. The stress-strain gradients through the HAZ are too steep and localized to be measured through traditional tensile testing, and are not accurately obtained through instrumented normal indentation [6]. Therefore, the testing procedure for weld characterization using the prototype scratch testing device is an innovative method of evaluating the strength and ductility of welded connections, which is essential to the safety and function of any assembled structure. The scratch depth is on the order of tens of microns (μm), and therefore may be considered as a non-destructive method.

This thesis has been divided into three chapters. In Chapter 1, I will briefly provide a background for the development of reverse algorithms for predicting elastic-plastic properties from instrumented scratch testing. In addition, I will discuss the trends observed during scratch testing based on prior numerical and experimental work. Specific attention will be given to the effect of adhesive friction between the base material and scratch indenter. Lastly a comparison of normal indentation and scratch indentation will be provided to highlight several benefits of the scratch test and as justification for the design of the prototype device. For Chapter 2, I will detail the design and construction of the portable scratch testing rig. This section will include a

summary of the device objectives and several parameters that must be considered within the design. Chapter 3 will describe the results of experimental testing performed using the portable scratch testing device. A scratch will be performed through a welded connection to highlight the novel application of monitoring changes in both strength and ductility. Finally I will provide a discussion based on the observations from the initial scratch testing prototypes, and provide recommendations for future models.

Introduction – References

[1]. M. Dao, N. Chollacoop, K.J. Van Vliet, T.A. Venkatesh, S. Suresh, "Computational modeling of the forward and reverse problems in instrumented sharp indentation," Acta Materialia, vol. 49, pp. 3899-918, 2001.

[2]. S.C. Bellemare, M. Dao, S. Suresh, "The frictional sliding response of elasto-plastic materials in contact with a conical indenter," International Journal of Solids and Structures, vol. 44, pp. 1970-89, 2007.

[3]. S.C. Bellemare, M. Dao, S. Suresh, "Effects of mechanical properties and surface friction on elasto-plastic sliding contact," Mechanics of Materials, vol. 40, pp. 206-19, 2008.

[4]. S.C. Bellemare, M. Dao, S. Suresh, "A new method for evaluating plastic properties," Acta Materialia, vol. 58, pp. 6385-63892, 2010.

[5]. J.A. Williams, "Analytical models of scratch hardness," vol. 29, no. 8, pp. 675-95, 1996.

[6]. R.R. Ambriz, D. Chicot, N. Benseddiq, G. Memacque, S.D. De la Torre, "Local mechanical properties of the 6061-T6 aluminum weld using micro-traction and instrumented indentation," European Journal of Mechanics and Solids, vol. 30, pp. 307-15, 2011.

Chapter 1: Review of Material Testing Using Contact Mechanics

In this chapter, I briefly describe the historical research associated with scratch testing of materials. This includes the analytical framework for the dimensionless functions proposed by Bellemare *et al*. A summary of the trends and observations from scratch testing experiments and numerical simulations will also be provided. Finally, the scratch testing and normal indentation methods will be compared to highlight the benefits of scratch testing and to justify the design and construction of a portable scratch testing device.

1.1 Normal Indentation Testing

A normal indentation test consists of pressing a hard indenter into the surface of a softer material to determine its resistance to local deformation under an applied pressure [1,2]. The traditional definition of indentation hardness as measured from the residual deformed shape is,

Eq. 1.1: $$H_n = \frac{F_n}{A_r},$$

where F_n is the applied normal load, and A_r is the residual area of contact after the load is removed [1,3]. The use of the residual profile for determining the area of contact is justified provided that the ratio of elastic to plastic strains is small [4].

Indentation tests have been shown to be a measure of the plastic response of materials. During a normal indentation test, two different deformation modes may be observed, either sink-in or pile-up of material around the indenter. Materials which have a high ratio of yield stress to elastic modulus, σ_y/E, undergo significant elastic strains and will exhibit sink-in as the deformation is predominately distributed elastically throughout the material [4]. However, many engineering materials (and most metals) have a low ratio of σ_y/E, and therefore can be assumed to behave as rigid-plastic with significant plastic strain. These materials may exhibit either sink-in or pile-up depending on the strain hardening exponent, n of the material [1,4]. Pile-up is observed for materials which are either not hardening or have already been work hardened, and therefore have a low strain hardening exponent, n. Materials that are highly annealed or have a high value of n will exhibit sink-in. This is because work hardening of the material closest to the surface causes preferential strain of the material away from the contact interface, which is a similar observation to high σ_y/E materials.

Indentation hardness testing has been used for centuries, but more sophisticated instrumentation has allowed for the development of instrumented indentation. In instrumented indentation, the load-displacement hysteresis response is monitored during a normal indentation experiment. By monitoring parameters of these load-displacement curves, researchers have found methods of extracting mechanical properties of materials such as the Young's Modulus, yield strength, and strain hardening exponent [5,6]. Dao *et al.* proposed a method of deriving reverse algorithms to determine material properties for instrumented normal indentation tests [5]. Numerical tools like Finite Element Analysis (FEA) are used to obtain dimensionless functions that directly correlate characteristics of an experimental load-displacement curve with the yield strength and indentation hardness of a power-law hardening material.

1.2 Scratch Testing

Historically, scratch testing has been used as a method of semi-quantitatively comparing the hardness of materials (Mohs hardness scale) or tribological resistance. Tabor recognized that scratch testing, like normal indentation, was largely dependent on the plastic properties of the material [2]. Similar to normal indentation, the deformation modes during a scratch test can consist of either sink-in or pile-up based on the magnitude of the elastic strain (σ_y/E) and strain hardening exponent (n). These observations, and the work by Dao et al., led to Bellemare et al. determining the dimensionless functions relating measurements of the residual scratch profile to the yield strength and strain hardening exponent of power-law hardening materials [7].

1.2.1 Steady-State Instrumented Scratch Testing

The framework proposed by Bellemare *et al.* is applicable for power-law hardening materials which experience predominately plastic deformation. Specifically, the materials follow Hooke's law elasticity and von Mises yielding with isotropic power-law hardening where the true flow stress constitutive equation is given by,

Eq. 1.2: $$\sigma = \sigma_y \left(1 + \frac{E}{\sigma_y}\varepsilon_p\right)^n,$$

where ε_p is the true equivalent plastic strain, σ_y is the initial yield strength, E is the Young's modulus, and n is the plastic strain hardening exponent [7]. During contact, both the indenter

and material being scratched experience elastic strains which can be considered using an effective elastic modulus defined as,

Eq. 1.3: $E^* = \left[\frac{E}{(1-\nu^2)} + \frac{E_i}{(1-\nu_i{}^2)}\right]$,

where E_i and ν_i are the Young's modulus and the Poisson's ratio of the indenter, respectively [3]. Therefore, a material's stress-strain distribution can be defined by its elastic constants, yield strength, and strain hardening exponent. The theory assumes the use of a conical indenter with a total included angle of 140.6°, which has been shown to have the same area-to-depth ratio as the Berkovich three-sided pyramid and Vickers four-sided pyramid commonly used in normal indentation [8].

During a scratch experiment, a hard indenter is pressed into a softer material with a known normal load, F_n, in the same manner as a normal indentation test. Subsequently a tangential force, F_t, is applied parallel to the surface of the softer material. As the lateral load increases, the indenter begins to sink deeper into the material as contact on the back half of the indenter is lost and only the front half of the indenter is supporting the applied loads [3]. As displaced material flows upwards along the face of the cone, the indenter will begin to rise towards the undeformed surface. Eventually the indenter reaches a steady state where the depth of the indenter with respect to the undeformed surface remains constant. Under these conditions, the residual scratch profile will have a constant depth below the original undeformed surface, h_r, pile-up height above the original undeformed surface, h_p, and width, $2a_r$, which is the diameter of the profile measured between pile-up peaks, h_p [7]. The indenter geometry and free body diagram as well as the characteristics of the residual impression are shown in Figure 1.1. The characteristic dimensions as well as the applied normal load can be used to derive a normalized pile up ratio, r_p and scratch normal hardness H_s,

Eq. 1.4: $r_p = \frac{h_p}{h_r}$

Eq. 1.5: $H_s = \frac{F_n}{(\pi/2)a_r{}^2}$.

By definition, the scratch normal hardness is determined using only half of the apparent area of contact because the load is assumed to be supported only on the front face of the indenter while sliding. The correlations presented by Bellemare *et al.* are only appropriate for materials which exhibit pile-up deformation during a scratch experiment, because sink-in complicates the

measurement of the width of the scratch, $2a_r$. Also, note that Bellemare et al. finds that a steady state condition is reached that after the indenter travels a distance that is 2 to 3 times the width of the scratch, $2a_r$ [9].

Figure 1.1: Schematic of indenter and residual scratch profile geometry

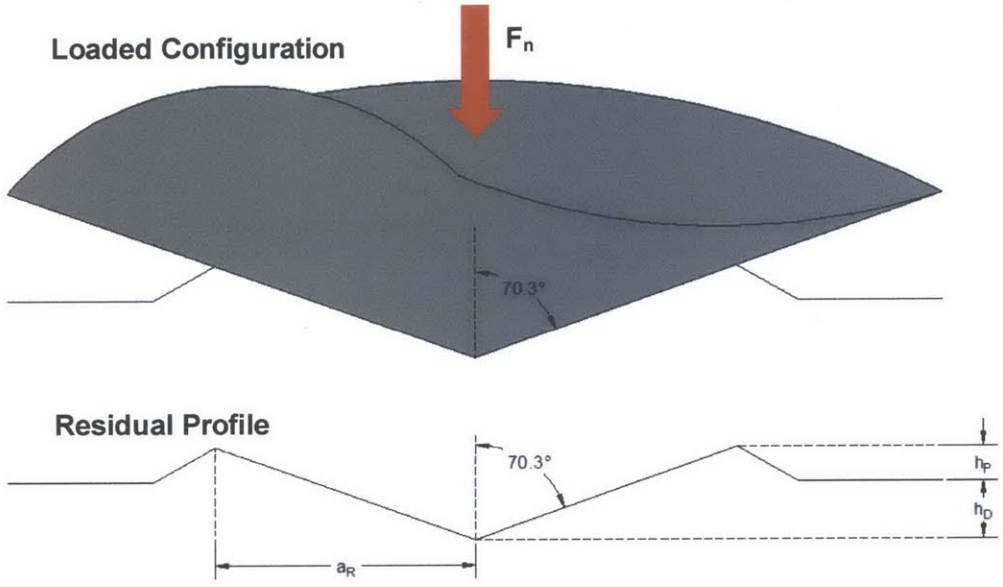

The Parameters identified in Eq. 1.3, Eq. 1.4, and Eq. 1.5, as well as the adhesive surface friction between the indenter and the material, μ_a, are input into dimensionless functions to obtain the tested material's yield stress and strain hardening exponent. These functions were derived by Bellemare *et al.* through the use of FEA and have the form [9],

Eq. 1.6: $$\Pi_\alpha(H_s, E^*, n, \mu_a) = \left(\frac{\sigma_y}{E^*}\right) = \left[\left(\frac{H_s}{E^*}\right)/(\alpha 1(n) + n\Gamma_{\alpha 1}(\mu_a))\right]^{[1/(1+\alpha 2(n)+\Gamma_{\alpha 2}(\mu_a))]},$$

Eq. 1.7: $$\Pi_\beta(\Pi_\alpha, n, \mu_a) = \left(\frac{h_p}{h_r}\right) = \Pi_{\beta,RP}(n)\Gamma_{\beta,RP}(\mu_a)/\left[1 + \left(\frac{\Pi_\alpha}{X_\beta(n)\Gamma_{X\beta}(\mu_a)}\right)\right]^{p_\beta(n)}.$$

These equations are applicable for a wide range of material properties which meet the following,

Eq. 1.8: $(4.8x10^{-5})n^{-1.22} < \left(\frac{\sigma_y}{E^*}\right) < (5.5x10^{-2})e^{-5.11n}$ where $0 \leq n \leq 0.5$.

The dimensionless functions can be plotted for a constant value of μ_a as shown in Figure 1.2, which was obtained with permission from Bellemare *et al* [9].

Figure 1.2: Chart for estimating material properties for $\mu_a = 0.15$

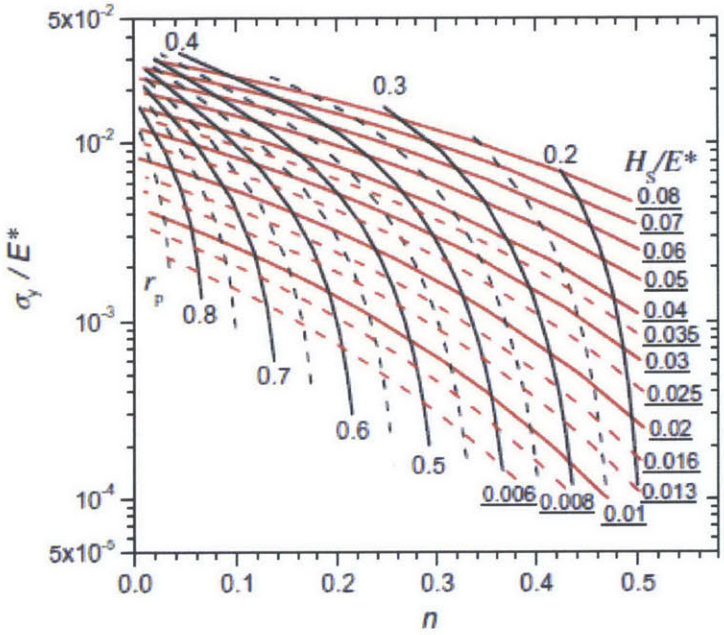

1.2.2 Role of Friction in Scratch Testing

During scratch testing, the total coefficient of friction, μ_{total}, is readily found by the ratio of the tangential force, F_T, to normal force, F_N. The total friction coefficient can then be decomposed into two terms as [10],

Eq. 1.9: $\mu_{total} = \frac{F_T}{F_N} = \mu_a + \mu_p,$

where μ_a is the adhesive surface friction from local interaction between the indenter and base material in normal contact, and μ_p is the ploughing friction due to the displacement of the softer base metal from the front of the scratch indenter. The adhesive friction μ_a is governed by the ratio of tangential to normal forces as stated by Amonton's law,

Eq. 1.10: $\mu_a = \frac{q}{p},$

where q is the tangential traction and p is the normal traction. Adhesive friction is dependent on the materials in contact and physical conditions of the local interface such as lubrication, asperities, and relative velocity [3,10,11]. To experimentally measure μ_a, multiple scratches

over the same area are performed with a spherical indenter causing the ploughing friction μ_p goes to zero, and the total friction, $\mu_{total} = \mu_a$, as shown in [12]. In general, the ploughing friction is dependent on the geometry of the indenter, depth of cut, and material properties [11]. However, for a conical indenter, the ploughing friction coefficient can be approximated for rigid-plastic materials by assuming a constant contact pressure as [10],

Eq. 1.11: $\mu_p = \frac{2}{\pi}\cot(\theta/2)$,

where $\theta/2$ is the half included angle of the indenter shown in Figure 1.1. This has been shown to be an upper bound solution in the absence of adhesive friction for rigid-plastic materials ($\sigma_y/E^* \leq 0.2$) through numerical analysis [13,14]. However, with increasing amounts of μ_a, μ_p will significantly deviate from the value predicted in Eq. 1.11 [12,13]. Wredenberg and Lasson suggest that the correlation is only appropriate if $\mu_{total} \leq 0.5$ [13]. The effect of adhesive friction on the ploughing friction term can be attributed to the change in depth of cut during the scratch testing experiment. As noted by Bellemare et al. [12] and predicted in analytical equations provided by Johnson [3], an increase in friction prevents the indenter from rising towards the surface when the tangential load is first applied, allowing the indenter to scratch at a greater depth which creates a greater contact area for a given load.

Having defined the parameters that define the frictional sliding response during scratch testing, the following trends have been determined through experimental and numerical observations:

- An increase in μ_a will cause an increase in μ_p as the depth of scratch increases [12,13].
- For $n < 0.35$, an increase in μ_a leads to a decrease in the scratch hardness [12]. As the scratch depth increases the residual width of the scar increases, decreasing the scratch normal hardness as shown in Eq. 1.5. Wredenberg and Larsson predict that the scratch hardness will decrease for any value of the strain hardening exponent [13,15], however, this observation was not validated through experimental testing like the results from Bellemare *et al* [12].
- For all values of n, an increase in μ_a causes an increase in the normalized pile-up height due to a deeper scratch depth and an increase in interaction forces along the face of the indenter [12]. For large values of μ_a, the increase in pile-up height and interaction forces may cause chipping or machining of the material [11], which prevents measurements of the ductile response from being obtained. Bellemare *et al.* limited the adhesive

coefficient of friction to 0.3 if $n \leq 0.2$, 0.2 if $n < 0.35$, or 0.3 if $n > 0.35$, to prevent instability in numerical simulations.

- For high values of total friction the shear forces necessary to plough through the material result in significant residual tensile stresses which may promote fracture of the material [13]. These observations have led to scratch testing being used as a method to extract the fracture toughness of various materials [16,17].

1.2.3 Trends observed during scratch testing of materials

Besides friction, there are several other parameters that effect the behavior of a scratch test. The following trends have been observed during scratch testing simulations and experiments which allow for a better understanding of the physical deformation processes during scratch testing:

- A decrease in strain hardening exponent causes an increase in pile-up height. This is because with less strain hardening there is more shearing deformation of the material contacting the indenter, and more material is displaced around the indenter as it slides. With more strain hardening, the deformation is distributed to a greater volume of material away from the contact interface [7].
- An increase in σ_y/E^* causes a decrease in pile-up height because of increasing levels of recoverable elastic strain [7].
- The pile-up response is much more dependent on the strain hardening behavior of a material than σ_y/E^*. In addition, yield strength effects the magnitude of plastic strain around the indenter while strain hardening effects the distribution of plastic strain throughout the underlying base material [12].
- The deformation mode changes from pile-up to sink-in when the strain hardening exponent increases to $n = 0.5$ and $\sigma_y/E^* > 0.005$ (significant elastic strain) [12]. This is consistent with the observations by others for both normal indentation and scratch testing [18,19].
- A smaller conical indenter included angle increases the risk of chip formation, but a larger included angle reduces the magnitude of plastic deformation [9]. This agrees with analytical models and experimental results reported by others [11].

1.3 Comparison of Scratch and Indentation Testing

After establishing the framework and behavior of instrumented scratch testing, we can now compare the method with instrumented normal indentation to highlight the benefits of a scratch testing experiment, and to justify the design and construction of a portable scratch testing device. As detailed below, a major advantage of scratch testing over indentation hardness is the increase in sensitivity to plastic strain properties.

1.3.1 Sensitivity and Accuracy of Analytical Functions

The normal indentation algorithms proposed by Dao et al. were verified using indentation experiments, and found that by averaging 6 indentation results the yield strength and indentation hardness can both be obtained within 10% of the actual value [5]. Individual measurements varied by as much as 40%. However, the reverse analysis functions were shown to be very sensitive to the input parameters, with a 4% variation causing up to a 96% change in the reported output. In addition, the algorithms predicts a unique solution for a limited range of materials with $n \leq 0.3$, and $\sigma_y/E < 0.03$ [7].

The scratch testing algorithms proposed by Bellemare et al. were shown to be less sensitive to experimental error, and cover a wider range of material properties as shown in Eq. 1.8. A 5% variation in one of the input properties of Eq. 1.6 and Eq. 1.7 leads to an error of at most 22% [9]. In addition, experimental results showed that 20 out of 22 cases covering a broad range of material properties were within 20% of the experimental data obtained from tensile test data, and all cases were with 38% [9].

In addition, a single scratch test can be used to collect hundreds of data points from the steady state profile which can be averaged to provide statistical confidence in the result. This allows for the scratch test to be a more time effective solution than normal indentation which requires multiple tests. Finally, the scratch testing algorithms are better suited for predicting the plastic strain hardening of a material. This is because the pile-up behavior during an instrumented scratch test is so strongly dependent on n. Another definition of n is the true plastic strain at which plastic instability occurs [20]. In a tensile test, this is observed as the plastic strain at the ultimate engineering stress where localized necking forms. Therefore, a good approximation of

n allows for relative comparisons of a material's ductility, a critical component of safe engineering design and re-ratings of existing structures.

1.3.2 Representative Strain

A useful concept that was developed early in the research on normal indentation is that of representative stress, σ_r, and strain, ε_r. These values are used to relate the stress-strain characteristics of a material with the indentation hardness. For fully work hardened materials ($n = 0$), Tabor established a relationship for normal indentation hardness,

Eq. 1.12: $H_N = C\sigma_y$,

where σ_y is the yield strength of the material, and C is a constant that is approximately 3 for rigid -plastic materials and is dependent on indenter geometry [2]. This relationship was derived from the observation that about 2/3 of the mean pressure during normal contact is due to hydrostatic pressure which does not contribute to inducing plastic flow. Tabor determined the constant, C, for various materials and indenter geometries in the fully work hardened condition, and found that the relationship could be extended to work hardening materials ($n > 0$) by replacing the yield stress with a representative stress, σ_r, as [1],

Eq. 1.13: $H_N = C\sigma_r$.

Using this correlation, Tabor found that the representative strain produced from normal indentation is independent of the strain hardening exponent and is between 8 and 10% [1]. Using the same definition as Tabor, Dao *et al.* determined a representative strain of 8.2% based on numerical modeling of 76 different material parameters [5]. Compare these representative strains from indentation to scratch testing, where Bellemare *et al.* determined a representative strain of 33.6% for materials with $n \leq 0.2$, or $n \leq 0.35$ and $\sigma_r/E < 0.018$ [7]. Similarly, Wredenberg and Larsson determined a representative strain of 35% using a conical indenter with a total included angle of 136° [13]. Therefore, the representative material strain produced during a single scratch experiment is 3 to 4 times greater than a normal indentation experiment, allowing for a greater understanding of the plastic response.

1.3.3 Correlation of Scratch Normal Hardness with Indentation Hardness

Tabor derived a ratio of scratch normal hardness to indentation hardness of 1.2 [2]. However, later studies have shown that there is no simple correlation between indentation and scratch hardness due to the different effects of friction and the more pronounced effect of strain hardening on the pile-up response. Wredenberg and Larson [13] used numerical simulations to find that the ratio of scratch hardness to indentation hardness converges to 1 for rigid-plastic materials in the absence of adhesive friction and with low strain hardening ($n \leq 0.17$). Experimental results showed that the ratio ranged from 1 to approximately 1.75 [15]. Prasad *et al.* reports that literature shows that the ratio ranges from 1.6 to 0.58, and used numerical results without adhesive surface friction to find values of 1.2 to 1.6 for various plastically graded materials [14]. Based on these observations, there is no straight forward correlation between scratch normal hardness and indentation hardness. However, using a similar approach taken by Bellemare et al., forward algorithms could be developed to directly relate the strain hardening and initial yield strength parameters to normal indentation hardness experiments. This work could provide a benefit to engineers who wish to compare the novel scratch testing method with existing non-destructive techniques.

Chapter 1 – References

[1]. D. Tabor, The hardness of metals. Oxford University Press; 1951. .

[2]. D. Tabor, "The physical meaning of indentation and scratch hardness," *Br J Appl Phys,* vol. 7, no. 159, pp. 159-66, 1956.

[3]. K.L. Johnson, Contact mechanics. Cambridge University Press; 1985. .

[4]. N.A. Stilwell, D. Tabor, "Elastic recovery of conical indentations," *Phys Proc Soc,* vol. 78, no. 2, pp. 169-79, 1961.

[5]. M. Dao, N. Chollacoop, K.J. Van Vliet, T.A. Venkatesh, S. Suresh, "Computational modeling of the forward and reverse problems in instrumented sharp indentation," *Acta Materialia,* vol. 49, pp. 3899-918, 2001.

[6]. J.L. Bucaille, E. Felder, G. Hochstetter, "Mechanical analysis of the scratch test on elastic and perfectly plastic materials with the three-dimensional finite element modeling," *Wear,* vol. 249, pp. 422-32, 2001.

[7]. S.C. Bellemare, M. Dao, S. Suresh, "The frictional sliding response of elasto-plastic materials in contact with a conical indenter," *International Journal of Solids and Structures,* vol. 44, pp. 1970-89, 2007.

[8]. A. Bolshakov, G.M. Pharr, "Influences of pileup on the measurement of mechanical properties by load and depth sensing indentation techniques," *Journal of Materials Research,* vol. 13, no. 4, pp. 1049-58, 1998.

[9]. S.C. Bellemare, M. Dao, S. Suresh, "A new method for evaluating plastic properties," *Acta Materialia,* vol. 58, pp. 6385-63892, 2010.

[10]. F.B. Bowden, D. Tabor, The friction and lubrication of solids. Oxford University Press; 1950. .

[11]. A.J. Black, E.M. Kopalinsky, P.L.B. Oxley, "An investigation of the different regimes of deformation which can occur when a hard wedge slides over a soft surface: The influence of wedge angle, lubrication and prior plastic working of the surface," *Wear,* vol. 123, pp. 97-114, 1988.

[12]. S.C. Bellemare, M. Dao, S. Suresh, "Effects of mechanical properties and surface friction on elasto-plastic sliding contact," *Mechanics of Materials,* vol. 40, pp. 206-19, 2008.

[13]. F. Wredenberg, P.L. Larsson, "On the numerics and correlation of scratch testing," *Journal of Mechanics of Materials and Structures,* vol. 2, no. 3, pp. 573-94, 2007.

[14]. A. Prasad, M. Dao, S. Suresh, "Steady-state frictional sliding contact on surfaces of plastically graded materials," *Acta Materialia,* vol. 57, pp. 511-24, 2009.

[15]. F. Wredenberg, P.L. Larsson, "Scratch testing of metals and polymers: Experiments and numerics," *Wear,* vol. 266, pp. 76-83, 2009.

[16]. A.T. Akono, N.X. Randall, F.J. Ulm, "Experimental determination of the fracture toughness via microscratch tests: Application to polymers, ceramics and metals," *J Mater Res,* vol. 27, no. 2, pp. 485-93, 2012.

[17]. F.J. Ulm, S. James, "The scratch test for strength and fracture toughness determination of oil well cements cured at high temperature and pressure," *Cement and Concrete Research,* vol. 41, pp. 942-6, 2011.

[18]. N.A. Stilwell, D. Tabor, "Elastic recovery of conical indentations," *Phys Proc Soc,* vol. 78, no. 2, pp. 169-79, 1961.

[19]. D.M. Marsh, "Plastic flow in glass," *Proc Roy Soc,* vol. 279, no. 18, pp. 420-35, 1964.

[20]. R. Hertzberg, Deformation and fracture mechanics of engineering materials. 4th ed. John Wiley & Sons, Inc.; 1996.

Chapter 2: Prototyping of Scratch Test Device

This chapter details the design, construction, and optimization of the scratch testing device. An initial prototype was able to validate the mechanics of the invention by ploughing a scratch at a constant depth through a high strength low-alloy steel material. However, following the development of the first prototype, the decision was made to construct a second prototype based on the lessons learned through the first which would be more suited for implementation by practicing engineers. The second prototype included more sophisticated instrumentation to ultimately allow the residual scratch parameters to be measured in-situ during a scratch experiment. A complete summary is provided below.

2.1 Design Constraints

To complete a scratch, the device will be subjected to forces normal and parallel to the surface of the test sample. For the scratch testing device to be practical in engineering applications, the size must be kept as small as possible such that it can be easily attached to larger structures and it can probe for material properties in confined areas. This section details the development procedure of the many components that make up the scratch test device.

2.1.1 Depth Control Mechanism

Using the instrumented scratch testing method developed by Bellemare et al. (Chapter 1), the mechanical properties of the material can be extracted by measuring the normal force on the indenter tip along with the dimensions of the scratch profile; specifically the depth, width, and pile-up height. However, we propose the use of an innovative displacement control procedure where the depth of penetration of the scratch indenter is constant, and the reaction force on the tip is monitored during the experiment. This is accomplished by using two supports, which are referred to as 'skates', which contact the test sample in the same plane as the indenter tip. The initial offset between the elevation of the skates and indenter tip effectively sets the depth of the scratch experiment. To maintain a constant depth, a normal load must be applied to the device that is greater than or equal to the reaction force on the tip, with the residual normal force applied being supported by the skates.

Existing laboratory scratch equipment utilizes a controlled normal load (Micro Materials, CSM Instruments). This force control method requires advanced measurement techniques such as

piezoelectric devices or profilometry to determine the depth of the scratch after an experiment. Using the depth control method reduces the number of experimental measurements necessary from 4 to 3, because the scratch depth is a known value. The initial scratch depth may be considered the same as the residual depth after elastic unloading, because the test materials are metals which experience significant plastic deformation (low σ_y/E^*). Considering the representative strain of 33.6% calculated by Bellemare et al., a typical structural steel or aluminum alloy will have an elastic strain of about 0.2%, which is less than 0.6% of the overall strain magnitude.

The number of variables that must be measured can be further reduced to 2 if you consider that the scratch profile will match the geometry of the indenter tip making the scratch. Therefore, if the angle of the conical indenter (θ) and the depth of the scratch (h_r) are known, only the width (a_r) or height of the pile-up (h_p) must be measured to fully describe the scratch profile through simple trigonometry. This concept is detailed in Figure 2.1. If local changes in material properties are desired, than the reaction force and scratch profile measurements must be correlated to the position of the indenter and scratch profile measurements along the length of the scratch.

Figure 2.1: Relationship between scratch profile measurements for given conical indenter

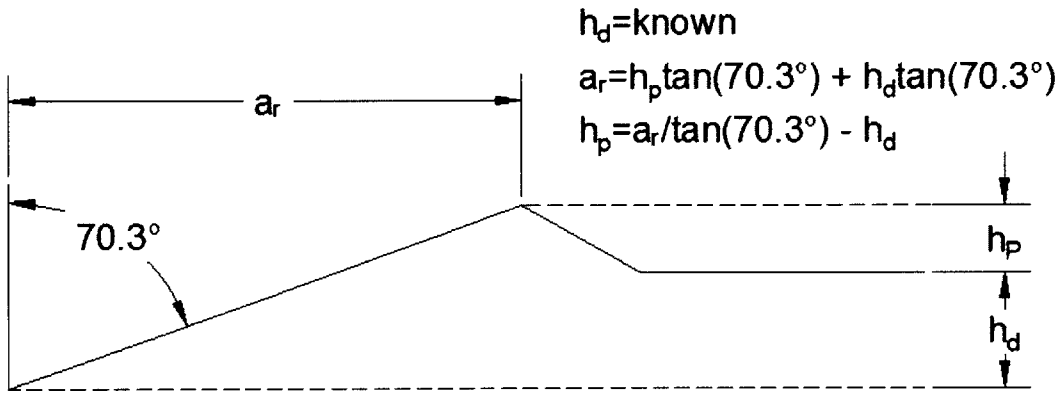

2.1.2 Depth of Penetration

As detailed in Chapter 1, the depth of a load control scratch experiment is dependent on the normal load applied, material properties, and frictional forces between the indenter and material. With a displacement control experiment, the depth of penetration is controlled only by the

relative adjustment of the contact points between the skates and the indenter tip, provided that the force applied is greater than the normal reaction force on the indenter. Any remaining normal force is resisted by the skates also contacting the test material, resulting in a constant depth of penetration. Surface preparation of the test sample is required to reduce the roughness of the material so that it will not affect the size of the scratch or subsequent measurements of the scratch pile-up height [1]. Therefore, a greater scratch depth, and consequently greater normal indentation reaction force, will reduce the amount of surface preparation required. The calculation of the penetration depth for a rigid body into an elastic-plastic medium is readily accomplished through numerical methods.

To estimate the reaction force for design, I utilized the Finite Element Analysis (FEA) software Abaqus to simulate normal indentation experiments with increasing load. Finite Element Analysis is a continuum mechanics numerical technique where a domain representing some spatial geometry is discretized into a mesh of smaller elements. Each element contains nodes where interactions between neighboring elements occur based on an assumed polynomial behavior. The nodal response is then calculated based on the stiffness matrix and external loading and boundaries defined by the user. With an appropriately sized mesh, the numerical solution will approach the exact solution of the simplified model [2].

I simulated two structural materials, a high strength low alloy steel and a tempered aluminum alloy. For both materials, an elastic-plastic true stress-strain curve was created assuming a simple power-law hardening behavior, as defined by [3],

Eq. 2.1 $$\sigma = K{\varepsilon_p}^n,$$

where, K is a strength coefficient, ε_p is the plastic strain, and n is the strain hardening exponent. The values of K and n were obtained from literature [4,5], and are presented in Table 2.1.

Table 2.1: Power-law material inputs representing common structural materials

Material	Strength Coefficient, K (psi)	Strain hardening exponent, n
4130 alloy steel	119,500	0.12
6061-T6 aluminum	59,000	0.05

The model consists of a rigid conical indenter being pressed into an elastic-plastic material under a normal load increasing from 0 to 50 lbs. To reduce the model size, a two-dimensional

axisymmetric model was used, which has been shown to be equivalent to the full three-dimensional domain by other researchers [6]. The length of the model is approximately 100 times the size of the indentation to ensure that the simulation represents local deformation of a bulk material. The surface boundary of the model was a free surface, the symmetry plane was an axisymmetric boundary, and the remaining boundaries were rollers to prevent lateral displacement of the bulk material. A refined mesh was used to model contact between the indenter and the material, and more than 30 elements were in contact with the indenter at maximum penetration. The model conditions are shown in Figure 2.2, as well as the von Mises stress field indicating localized stress near the contacting surfaces, and a close-up of the refined mesh at contact. The load-displacement curves for both materials are provided in Figure 2.3. The dashed lines indicate results from a simulation with almost half as many elements in contact with the indenter, and the agreement between the two conditions indicates that the mesh is well converged.

Figure 2.2: Equivalent von Mises stress plot indicating model boundaries and mesh at contact

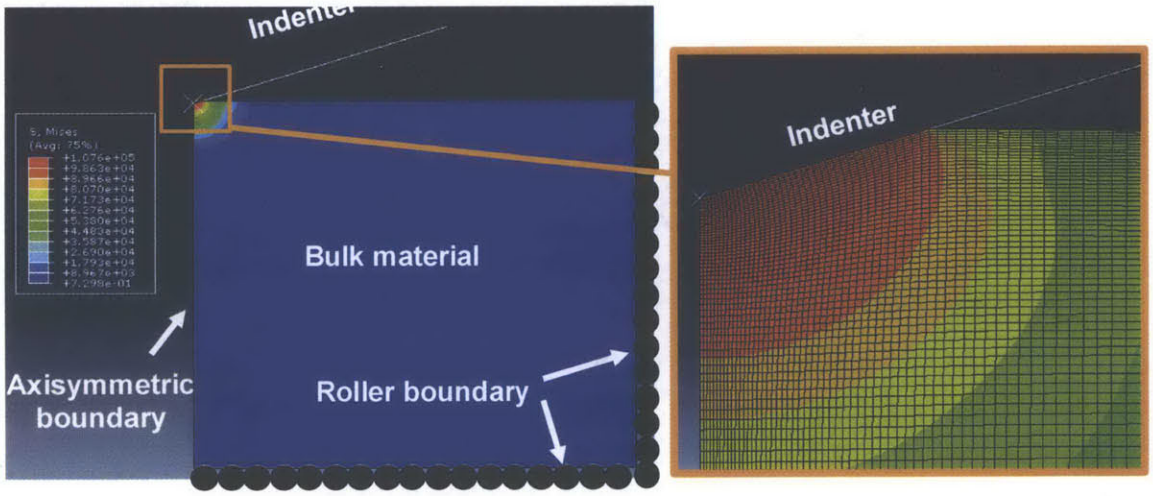

Figure 2.3: Load-displacement curves output for a structural steel and aluminum

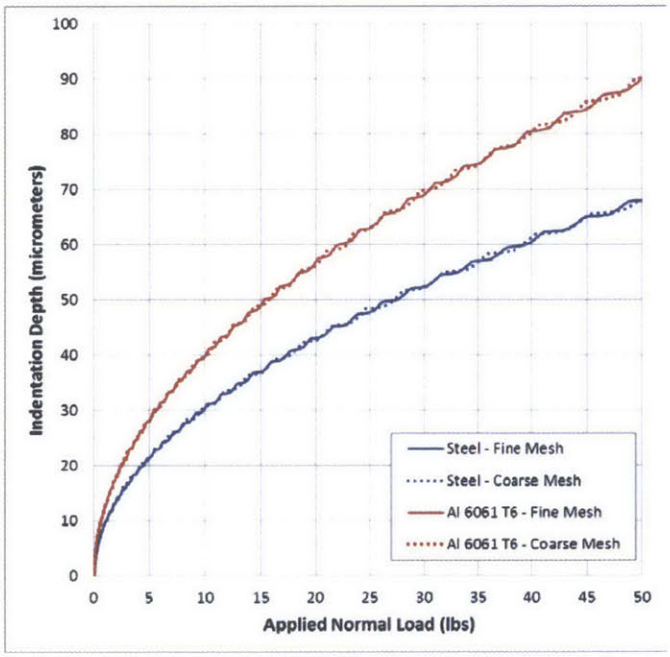

Based on the results shown in Figure 2.3, it was decided to design the scratch testing device to apply a normal force of 35 lbs to the indenter column to achieve a scratch depth of greater than 50 micrometers in a high strength material.

2.1.3 Load Application

A compact method was required to provide relatively large loads given the constrained size limitations of the device. After considering methods such as dead weights and electric motors, it was decided to use a double torsional spring to apply the normal load to the device. The torsional spring would be preloaded at one end, with the torsional moment applied to the device through a contact point on an intermediate load beam. Linear bearings were used to isolate the applied force on the device from the preload force on the spring, as well as to protect the motor that would be used to apply the ploughing force parallel to the surface of the test material. The axis of the double torsional spring also allowed for a pin connection between the scratch testing device and load assemblies, providing an internal hinge to simplify evaluation of the normal forces at contact.

Torsional spring design must consider the relatively high loads and the limited room for rotational preload. Steel music wire (ASTM A228) was selected due to its high tensile strength

and Young's modulus. We selected a double torsional spring that provided a torsional spring constant of approximately 1.1 lb-in. per degree rotation. The maximum allowable rotation was calculated as 38 degrees for a maximum torsional moment of 84 lb-in. This was based on the recommended ultimate tensile strength and safety factor provided by the spring manufacturer [7], and a stress concentration factor calculated based on analytical methods detailed by Shigley [8]. A lever was constructed for preloading the spring by threading a plate to the longest legs of the spring. The plate contained a circular hole that accommodated a one-quarter in. threaded rod with a nut and oversized washer. By raising the height of the nut and washer assembly on the threaded rod, a constant preload force could be applied to the spring, which is then transferred to the scratch test device.

The ploughing force must overcome the frictional force between the indenter tip and skates contacting the sample material, but must also be at a constant velocity to consider the experiment as quasi-static and minimize dynamic effects. After a review of available methods, a linear actuator utilizing a 0.222 in. diameter Epicyclic Ball Screw powered by a 12 volt DC motor with a 19:1 gear ratio was obtained. The actuator provides precise linear motion at a constant velocity, and is rated for a dynamic load of 40 lbs and a static load of up to 240 lb. For experiments, the motor velocity should be as low as possible while still providing enough force to overcome friction and plough the scratch through the test sample.

2.1.4 Selection of Indenter Tip Geometry and Material

In order to utilize the dimensionless functions determined by Bellemare et al. (Eq. 1.6, Eq. 1.7) the same indenter tip geometry must be utilized. Any modification would require the reconstruction of the dimensionless functions through reverse algorithms due to the effect on both the scratch hardness and scratch profile. For the high loads and greater depths of penetration that the device is designed for, suitable diamond scratch tips were not commercially available. Therefore, a suitable material must be chosen that provides high hardness and acceptable wear performance, as well as a sufficiently small grain size to minimize the effect of surface roughness on the measurement of the scratch profile. We selected a Tungsten Carbide with 12% Cobalt binder and reported transverse rupture strength of over 500,000. The tip was manufactured through wire Electrical Discharge Machining to the specified angle with a tolerance of plus or minus 0.5 degrees. For the tip chosen, the maximum allowable height of pile-up plus scratch depth would be 284 microns.

The tungsten carbide material has a considerably higher coefficient of friction than diamond during scratch experiments. Bellemare et al. [9] used repeated scratches to determine the adhesive coefficient of friction between the scratch indenter and sample material. Using the definition of total friction defined in Chapter 1 ($\mu_{total} = \frac{F_T}{F_N} = \mu_a + \mu_p$), the ploughing friction coefficient, μ_p, will reduce to zero with repeated scratches because there will be a decreasing magnitude of plastic deformation within the scratch profile, and the remaining friction component will be due to only adhesive friction. Experiments were conducted with a spherical tungsten carbide ball indenter and 5 Newton normal load using a commercial nano-indentation testing device (Nanotest, Micro Materials Ltd., Wrexham, United Kingdom). Results for a typical experiment are shown in Figure 2.4, with a constant adhesive friction coefficient obtained after roughly 8 passes of the scratch indenter. The average adhesive friction coefficient from 4 sets of friction scratch experiments is 0.345. Compare this number to the value of 0.14 reported by Bellemare et al [9] using a diamond indenter. As discussed in Chapter 1, the greater coefficient of friction will lead to greater pile-up height ratios and increase the risk of forming chips during the experiment. For this reason, a lubricant must be used for all tests performed to decrease the adhesive component of friction.

Figure 2.4: Results of frictional scratch experiments with a tungsten carbide indenter

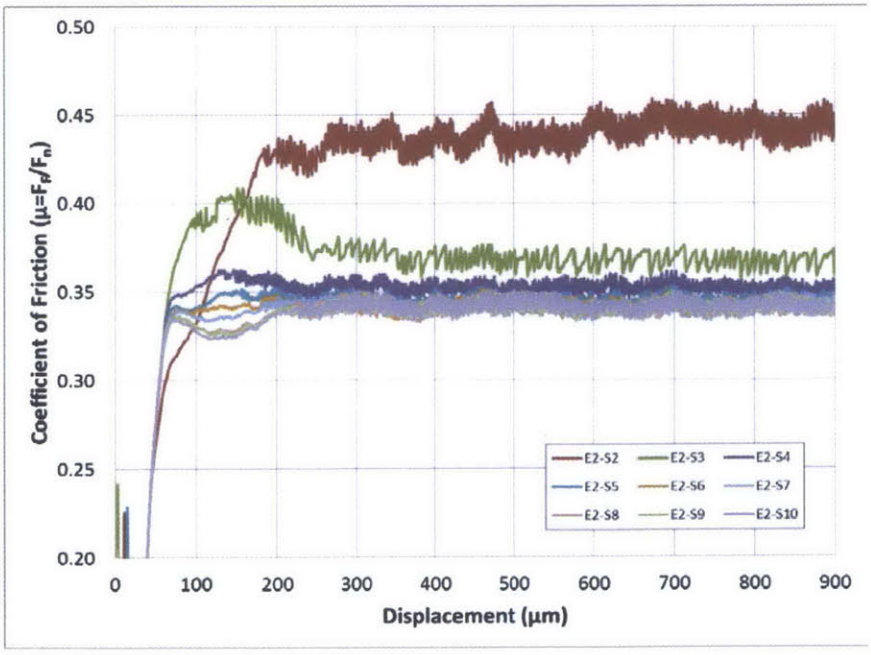

Table 2.2: Friction coefficient obtained from repeated scratch experiments

Scratch No.	Experiment Number				Average
	1	2	3	4	
1	Steady state not reached				
2	0.449	0.411	0.411	0.399	0.418
3	0.371	0.368	0.372	0.369	0.370
4	0.355	0.352	0.354	0.356	0.354
5	0.344	0.345	0.348	0.351	0.347
6	0.339	0.342	0.347	0.35	0.345
7	0.338	0.342	0.347	0.351	0.345
8	0.337	0.342	0.348	0.351	0.345
9	0.337	0.342	0.348	0.352	0.345
10	0.337	0.342	0.349	0.352	0.345

As detailed in Chapter 1, the effect of friction must be carefully considered during a scratch experiment. For high values of friction, the significant interaction forces between the indenter and test material leads to greater pile-up ratios and may cause chipping. Chipping of the test material prevents accurate measurement of the ductile properties using the instrumented scratch test method. Therefore, an appropriate lubricant must be selected. A sample of Iso-stearic acid was obtained from Nissan Chemical. The lubricant has a viscosity of approximately 141 centipoise at 20°C. A similar compound was shown to decrease the coefficient of friction by up to 25% in experiments conducted by Bellemare et al. with a diamond indenter [9].

2.1.5 Support system

A testing rig was constructed to perform the instrumented scratch experiment and to protect sensitive components. To protect the motor and to separate the torsional spring preload and resultant forces, two linear bearing pillow blocks were used. The linear bearings allow for low friction translational motion from the linear actuator motor while resisting significant radial loads applied through the torsional spring assembly. The linear bearings and motor assembly were bolted down to an aluminum plate to ensure proper alignment and to avoid eccentric loads on the motor assembly. A one-half in. diameter rod was used to travel through the linear bearings and connect the motor to the torsional spring loading assembly. The spring was joined to the one-half in. rod through a pin connection, with one side of the spring's legs extending back towards the motor for preloading, and the other legs extending out towards the scratch testing device to apply the normal load during experiments. The legs extending towards the scratch

testing device contacted another load beam where both the normal force and ploughing force were ultimately transferred to the device. The test location consisted of a plate with slots to accommodate clamps for securely holding sample materials for scratch testing. The height of the beams connecting to the indenter column were set by the linear bearings at 0.6875 in. During a scratch experiment, the ploughing force effects the normal force applied to the indenter column based on the direction of the scratch experiment. For a pushing direction, the indenter force will be increased by the moment generated between the sample surface, and for a pulling direction the indenter force will be decreased. Figure 2.5 provides an overview of the full testing assembly.

Figure 2.5: Image of the full testing assembly

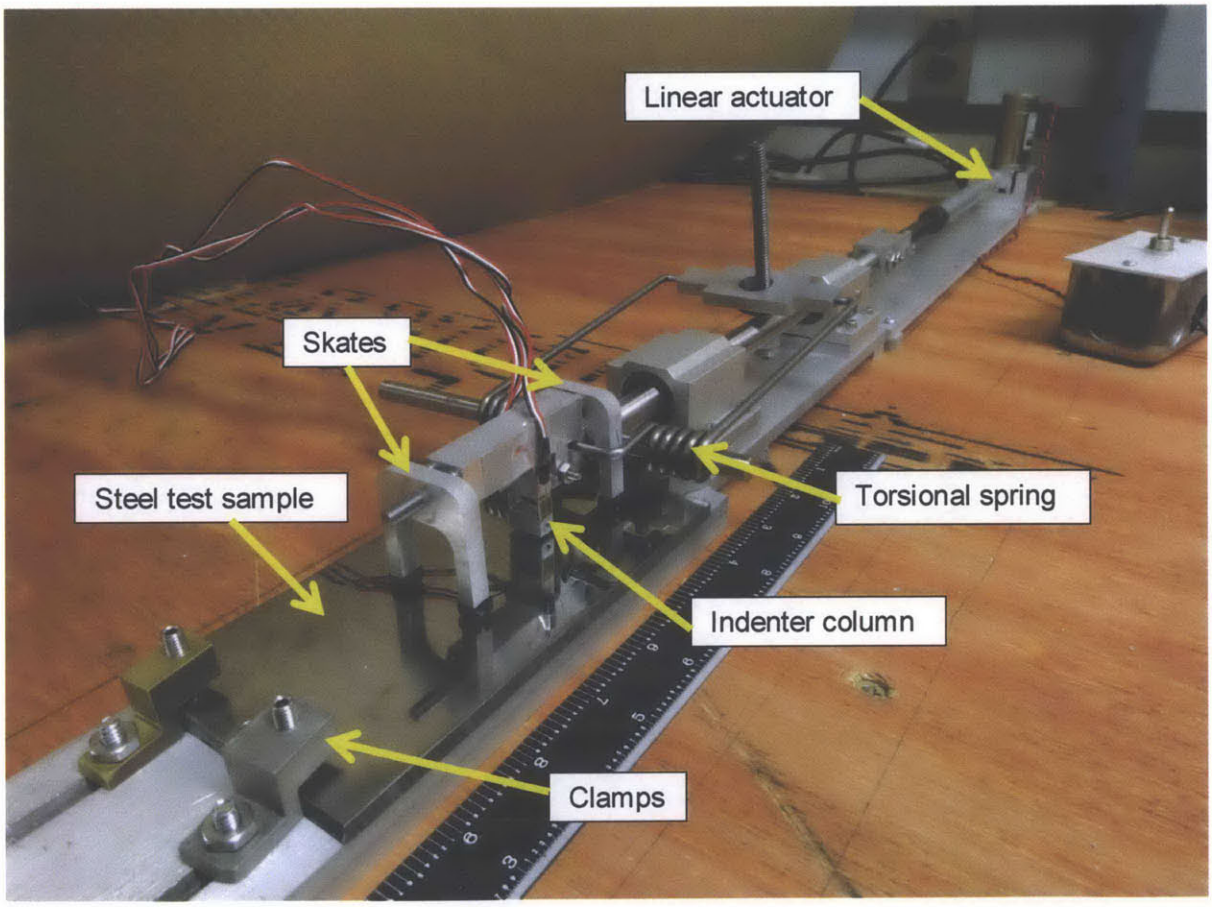

2.2 First Scratch Test Device Prototype

With these design constraints in mind, the first prototype design consisted of a main beam with a column supporting the indenter, referred to as the indenter column, close to the mid-span. On either end of the beam were two pairs of skates which provided additional points of contact with the test sample. The front pair of skates was connected with a journal bearing assembly to permit rotational motion of the legs for uneven surfaces. The rear pair of skates which was closest to the indenter was fixed to be a rigid assembly with the indenter column, allowing for implementation of the depth control mechanism. Both normal and ploughing forces were applied to the device at a pin attachment point located adjacent to the indenter column. For this design, the scratch test was performed with a pushing force which provided additional load to the indenter column due to the moment between the test sample surface and centerline of the loading beam axis. A photograph of the first prototype connected to the support system is shown in Figure 2.6

Figure 2.6: Photograph of first prototype design

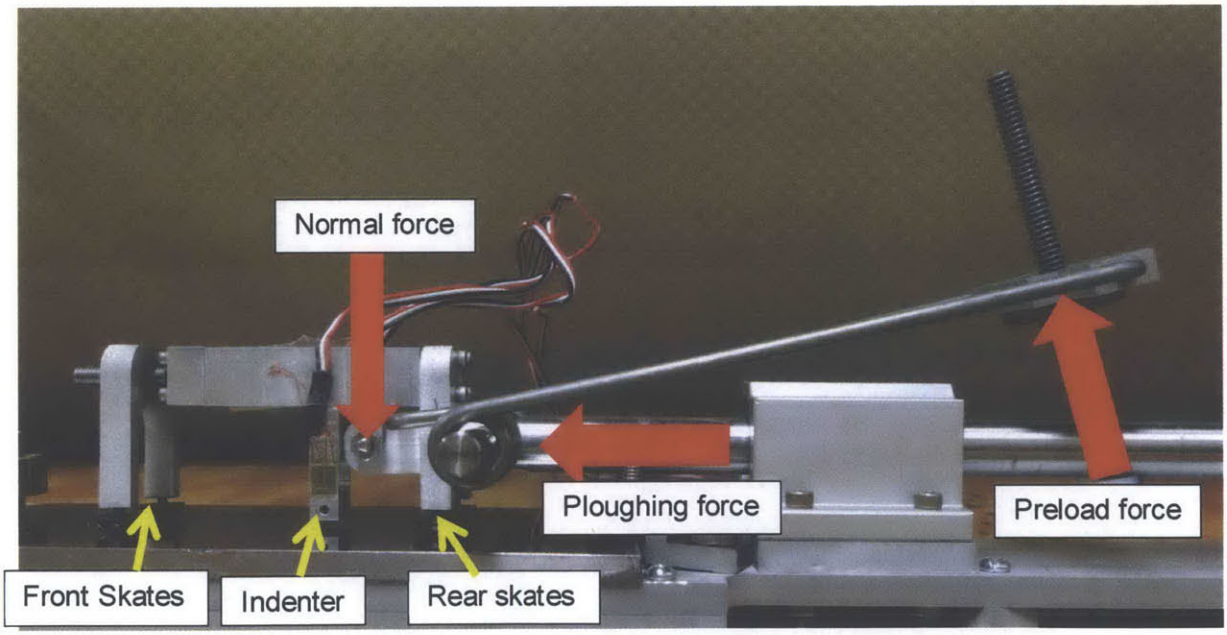

2.2.1 Validation of Depth Control Function

The first prototype and testing rig were used to conduct initial experiments on a 4130 high strength low alloy steel. The sample materials were ground using a polishing wheel up to 800

grit SiC paper to allow the scratch to be clearly visible after testing. Following testing, the scratch profile was examined using a Hirox digital microscope. The digital microscope is capable of stitching multiple two dimensional images together to form a three dimensional data file, allowing for measurements of the profile dimensions with a resolution of approximately 1 micron [10].

Figure 2.7 shows a two-dimensional image of the scratch taken at 700x magnification. Figure 2.8 shows the three-dimensional data file obtained from the stitched images, as well as a cross-sectional rendering through the scratch. The scratch cross-section indicates that the scratch is well formed with peaks at the same elevation. Several lengths of scratches were analyzed to compare the scratch depths and pile-up heights to confirm the depth control function of the device. These measurements were taken near the beginning, middle, and end of an approximately 25 mm long scratch. The entire scratch profile could not be imaged by the digital microscope, so portions of various lengths were imaged and then analyzed. For each length, 5 measurements were taken at equal intervals along the length examined to be averaged and compared. The results are shown in Table 2.3. Lengths 1 and 2 were after approximately 5 mm of scratch travel, 3 and 4 were after approximately 15 mm, and length 5 was after approximately 20 mm.

Figure 2.7: Two-dimensional image obtained from digital microscope (700x mag.)

Figure 2.8: Three-dimensional image file obtained from digital microscope (700x mag.)

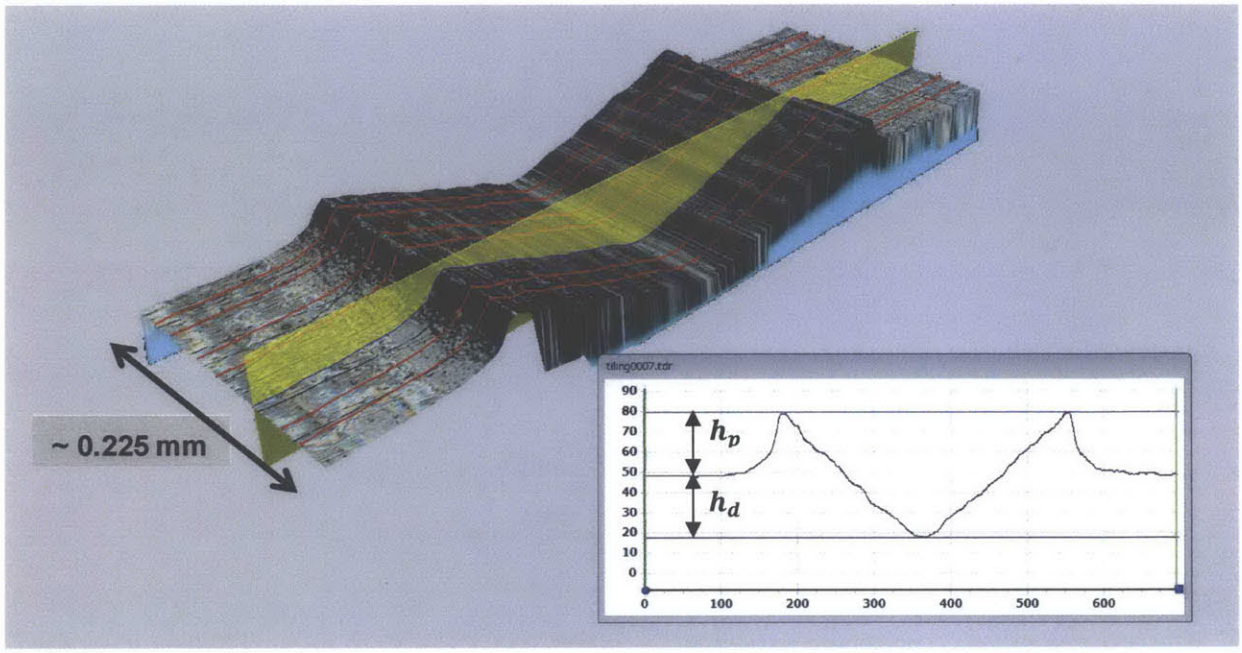

Table 2.3: Summary of measurements taken from digital microscopy

h_d = scratch depth, h_p = pile-up height, all measurements in micrometers

Profile #	L1 (150 um)		L2 (225 um)		L3 (225 um)		L4 (1400 um)		L5 (1400 um)	
	h_d	h_p	h_d	h_p	h_d	h_p	h_d	h_p	h_d	h_p
1	32.0	30.8	32.2	30.9	29.1	26.1	29.1	28.2	31.9	26.1
2	32.3	30.1	32.4	30.1	28.7	25.9	31.0	26.7	29.5	27.0
3	33.4	28.7	32.1	30.3	28.6	26.7	32.7	27.4	30.9	27.2
4	31.5	31.3	31.3	30.6	28.7	27.1	32.1	26.7	28.2	25.9
5	32.3	31.1	31.0	32.7	29.7	25.6	31.2	28.6	31.8	28.8
Avg	32.3	30.4	31.8	30.9	29.0	26.3	31.2	27.5	30.4	27.0
Stdev	0.7	1.0	0.6	1.1	0.5	0.6	1.4	0.9	1.6	1.1

The results from the scratch experiment validate that the depth control mechanics were able to successfully maintain a scratch of approximately constant depth. The standard deviation for all of the scratch depths measured was 1.5 micrometers, which is low compared to the plus or minus 1 micrometer resolution of the digital microscope. The standard deviation for the pile-up height was 2.1 micrometers, indicating that there is greater variability in the pile-up height than the scratch depth. This observation emphasizes the need for averaging measurements over a finite length for confident results.

2.3 Second Prototype Development

The initial prototype provided an opportunity to validate the depth control mechanism, a major innovation for the portable scratch tester. However, for the device to be utilized in a field environment for in situ scratch experiments, the device would need further optimization. These modifications include:

1. Optimize the geometry of the indenter column to maximize the amount of axial strain while still being strong and rigid in bending.
2. Reduce the overall length of the device to allow the test be conducted near corners or complicated geometries. These locations are common stress risers which necessitate careful consideration by engineers.
3. Move the skates to the same plane as the indenter tip during a scratch experiment. The skates should be fixed with respect to the indenter tip, but the entire assembly should be able to rotate to accommodate changes in slope of a test piece. With this modification, only one pair of skates is necessary.
4. Incorporate instrumentation within the scratch test device to continuously measure the scratch profile and reaction force during a scratch experiment. This development will greatly simplify the testing method and allow for quick post-processing of data.

2.3.1 Instrumentation

As discussed in Section 2.1.1, a displacement-controlled scratch test requires two measurements for inputs into the dimensionless functions developed by Bellemare et al. The first input is the reaction force (F_n) at the indenter tip, and the second is either the scratch width (a_r) or pile-up height (h_p) which can be used along with the known scratch depth (h_d) to fully describe the residual scratch profile (reference Figure 2.1). Ideally, these measurements will be obtained during a scratch experiment to maximize the practicality and usability of the testing method. Existing methods require the use of profileometry or optical techniques such as a digital microscope to obtain measurements of the scratch profile after a test has been completed. This information takes additional time to obtain, and processing the data to correct for sample slope and average pile-up height is time consuming.

2.3.1.1 Normal Force

The reaction force at the indenter tip can be obtained through strain gages attached to the indenter column. Strain gages are attached with an adhesive that must be carefully selected based on service conditions. When the device is loaded, strain on the surface is transferred to the strain gage through the bonded connection. The physical strain is related to changes in resistivity across a circuit by the Gage Factor, which relates fractional changes in resistance to fractional changes in strain [11]. To increase the sensitivity of strain measurements, we will utilize one of the most common electrical configurations, the full Wheatstone bridge, consisting of four active strain gages. Temperature effects are minimized by the use of three wire circuits for each individual strain gage (quarter bridge). During experiments, the combination of measured axial and bending strains in the column can be used to calculate equivalent axial loads through either Hooke's law for isotropic materials or empirical correlations to experiments.

The size and orientation of strain gages must be selected based on the desired application. Strain gages provide a measure of the average strain along their length, and therefore a relatively uniform strain gradient and sufficiently large gage area is need for accurate results [12]. However, the gage must also be relatively small to accommodate the compact geometry of our indenter column. For our application, we choose to utilize stain gages that are approximately 0.125 in. long, which is roughly 20% of the length of the column supporting load, and deserves special consideration detailed in Section 2.3.2. The gages would be oriented at approximately the same distance along the length of the beam, with two gages on both the tension and compression side of the indenter column. We utilized general purpose strain gage matrices containing 2 parallel gages (Omega Engineering) which were be bonded to opposite sides of the testing device using a general purpose laboratory adhesive (MBond 200, Micro-Measurements). The gages contained lead ribbons which would be soldered to bonded terminals to maximize the life of the system and prevent accidental loading through the wire attachments. The entire system was coated with a polyurethane lacquer for moisture resistance (HBM).

2.3.1.2 Scratch Profile

To define the scratch profile, the pile-up height or scratch width must be determined. We considered various methods including optical techniques such as pixel counting, non-contact inductive methods, and mechanical contact. The most significant constraint was the resolution of the measurement technique which must be very precise to measure small variations along

the scratch length. Ultimately we selected an ultrahigh precision gaging Linear Variable Displacement Transducer (LVDT) to measure the pile-up height through mechanical contact (MacroSensors). The LVDT provides a repeatability error of less than 0.15 micrometers, and utilizes an inner spring to maintain contact with the scratch profile.

The advantage of mechanical contact is that a stiff 'contact beam' could be attached to the bottom of the LVDT to measure material pile-up on both sides of the scratch, effectively averaging the two values without any post-processing. However, this effect requires the implementation of a miniature system of bearings to allow the contact beam to freely rotate from the torque generated by the spring force and the moment arm associated with the width of the scratch. In addition, the load applied by the spring force as well as the self-weight of the LVDT piston will induce some compression of the pile-up height. This effect can be accounted for using a correction factor. The lowest spring stiffness commercially available was obtained to limit the correction factor, and a normal load of approximately 30 grams was measured within the range of extension used for our application.

2.3.2 Design of Indenter Column

The indenter column must be designed to resist the normal and friction reaction forces at the tip of the indenter and must securely hold the indenter tip. In addition, the column must allow for as much axial strain as possible so that the normal force at the tip can be accurately obtained with strain gages. This may be accomplished by designing a section of the column to have a reduced cross-sectional area to promote axial strains. The reduced section must still be stiff in bending with a sufficient factor of safety against yielding. From a structural mechanics perspective, the indenter column may be considered as a cantilever beam-column, and therefore the reduced section should be as close to the test sample surface as possible to minimize the applied moment from friction. A last constraint is that the distance between the indenter tip and LVDT assembly that is measuring the scratch profile should be minimized. As the distance between the tip and LVDT increases, a longer scratch will be required in order to make measurements. For this reason, it was decided to offset the position of the indenter tip within the column. This creates an eccentric axial load, meaning that both an axial force and bending moment will be applied from the normal load, in addition to the shear and moment applied from the frictional force generated during the scratch experiment.

Different indenter column geometries were investigated to determine the optimum shape for the given constraints. For geometries stiff in bending, a rectangular or I-beam shape are natural first selections. For our application, the rectangle could be hollowed out to reduce the cross-sectional area and maximize the axial strain. Likewise, the I-beam would have thin flanges on its outer fibers and central web to decrease the cross-sectional area. To compare the two geometries, a Finite Element Analysis (FEA) was performed using the software Abaqus. The FEA model allows for the evaluation of stress concentrations at the reduced cross-section with a linear elastic material model, and for an examination of the stain gradient near the strain gage location. As discussed above, the strain gages should be applied in a relatively uniform strain field for consistent and accurate readings. For all models created, a normal load of 35 lb and a frictional force of 28 lb (assuming $\mu_{total} = 0.8$) were applied to the location of the indenter tip. The load was applied through a coupling constraint which maps the kinematic degrees of freedom of the bottom surface of the indenter column to a single reference point where the loads were applied [13]. The use of the coupling constraint prevents numerical difficulties associated with concentrated load applications at the point of contact.

The overall dimensions of the columns were rectangular with a depth of 0.25 in. for the uniaxial bending direction. All geometries considered the indenter tip offset a distance of 0.0835 in. from the neutral axis of the beam, or one third of the beam depth. The length of the indenter column was 0.6875 in., which is the length from the top surface of the scratch sample to the centerline of the loading beam as constrained by the support structure detailed in Section 2.1.5. The boundary condition at the centerline height was a fixed constraint to resist axial loads, shear, and moment. The position of the reduced cross section was located approximately 0.25 in. from the indenter tip, to provide sufficient room for the 3/16 in. long indenter tip to be embedded within the column. The total length of the reduced section was made to be 0.25 in. to provide sufficient room for the strain gages to be installed. For both geometries, the specific dimensions of the reduced cross-section were chosen such that at least 200 microstrain was achievable from the axial load of 35 lb, assuming a modulus of elasticity in compression of 10.2×10^6 psi for 6061-T6 aluminum [14]. The greater the magnitude of microstrain the more accurately the reaction force on the tip can be determined due to the effective resolution of the strain gages and data acquisition equipment.

For the rectangular section, a two-dimensional plane stress model utilizing reduced integration elements was constructed as shown in Figure 2.9. Reduced integration elements are known to be well suited for evaluating bending stress without the effects of shear locking [13]. Various

radii of 1/32 in. and 1/16 in. were investigated for the corners of the pocket, knowing that the stress concentration at these locations would decrease for a larger fillet radius. The width of the beam (into the page in Figure 2.9) was chosen as 0.25 in., and the thickness of the beam at the reduced cross-section was set at 0.03 in to meet the minimum axial microstrain requirement. The principal stresses in the direction of the longitudinal axis are plotted in Figure 2.11 for the model with the smallest pocket radius. The results show that a significant stress concentration exists at the reduced section, as well as a very high gradient in stress and strain. The top surface of the beam, which would be completely in compression if there was no stress riser, has both tensile and compressive strains within the anticipated strain gage region, and therefore is not suitable for our application.

Figure 2.9: Two-dimensional FEA model of hollow rectangular indenter column

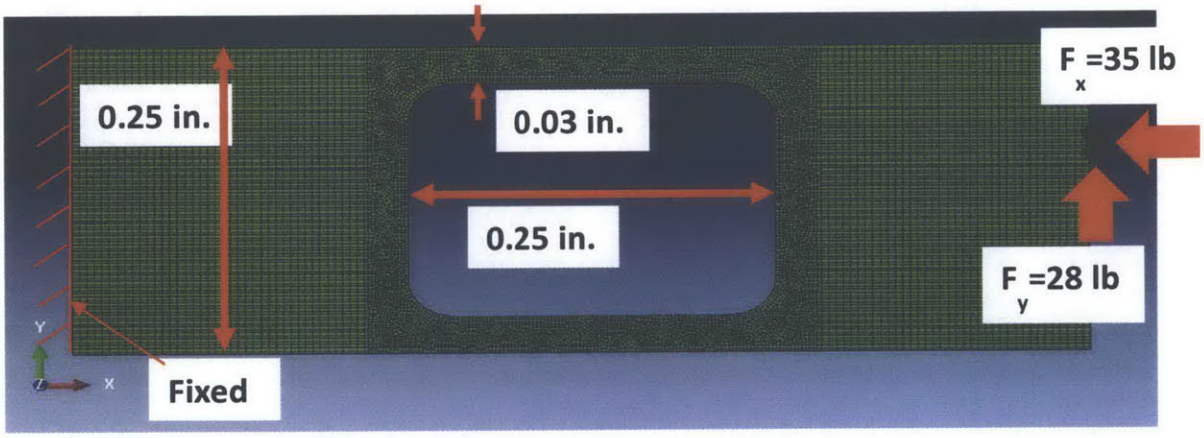

Figure 2.10: Principal axial and bending strains for rectangular indenter column (small radius)

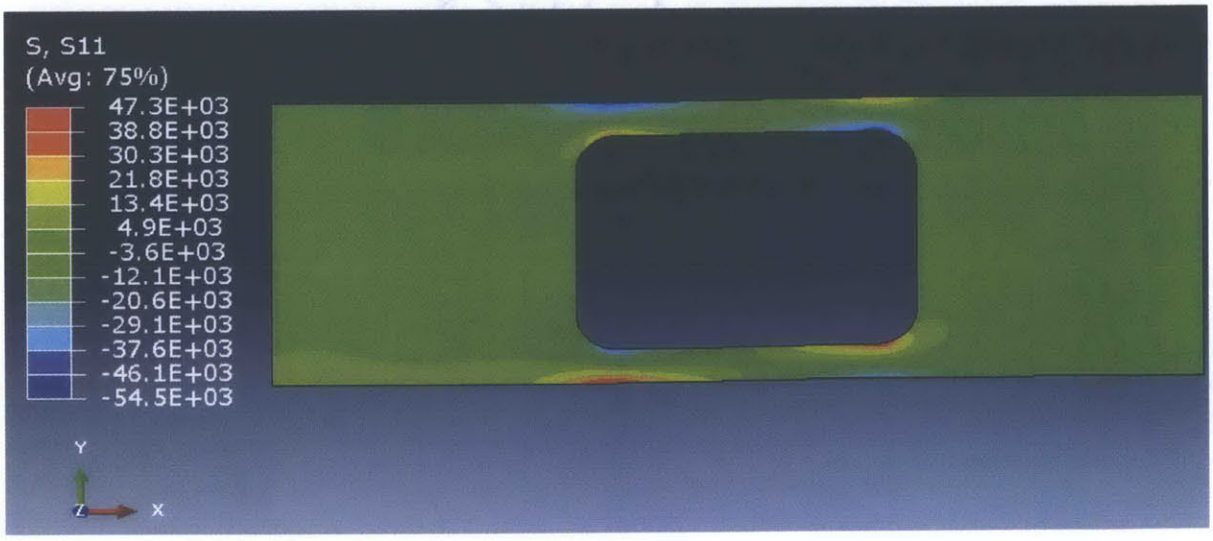

For the I-beam section, a three-dimensional FEA model was required as shown in Figure 2.11. Full three-dimensional stress elements with reduced integration were used to evaluate the axial and bending stress. Similar to the rectangular cross-section, radii of 1/32 in. and 1/16 in. were investigated for the corners of the pocket. The width of the beam was chosen as 0.25 in., and the thickness of the flange and web were set at 0.02 and 0.03 in., respectively. These dimensions met the minimum axial microstrain requirement while still being large enough to be machined using a three axis Computer Numerically Controlled (CNC) end mill. The principal stresses in the direction of the longitudinal axis are plotted in Figure 2.12 for the model with the smallest pocket radius. The results indicate a low stress concentration and a relatively smooth stress-strain gradient.

Figure 2.11: Three-dimensional FEA model of I-beam indenter column

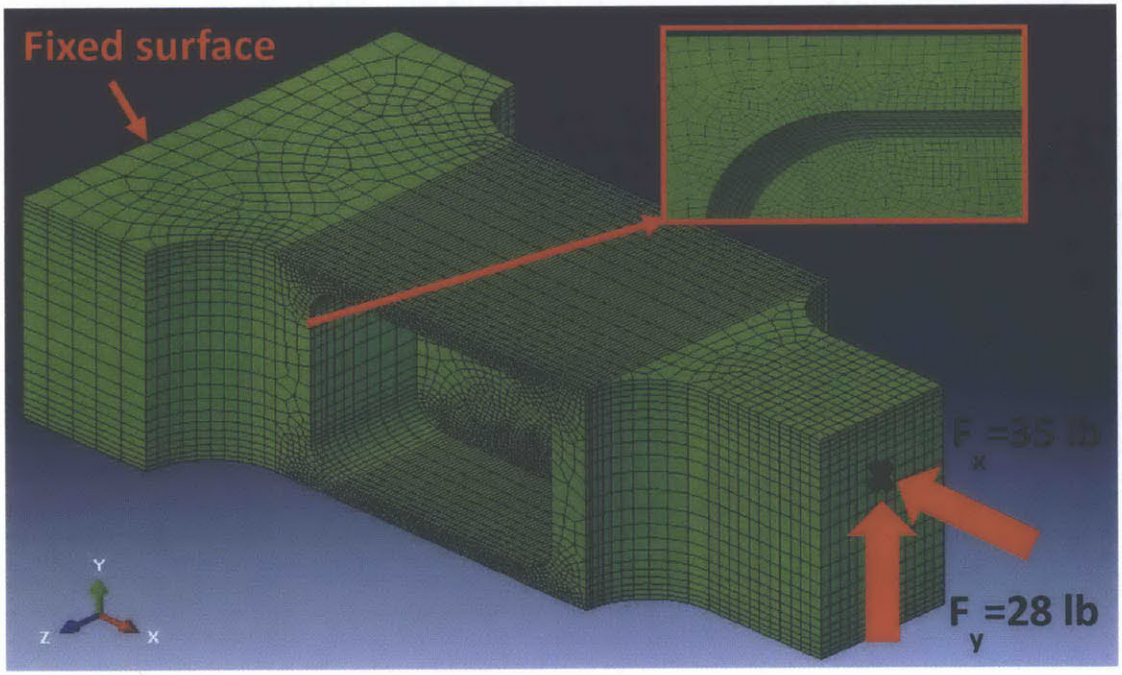

Figure 2.12: Principal axial and bending strains for I-beam indenter column (small radius)

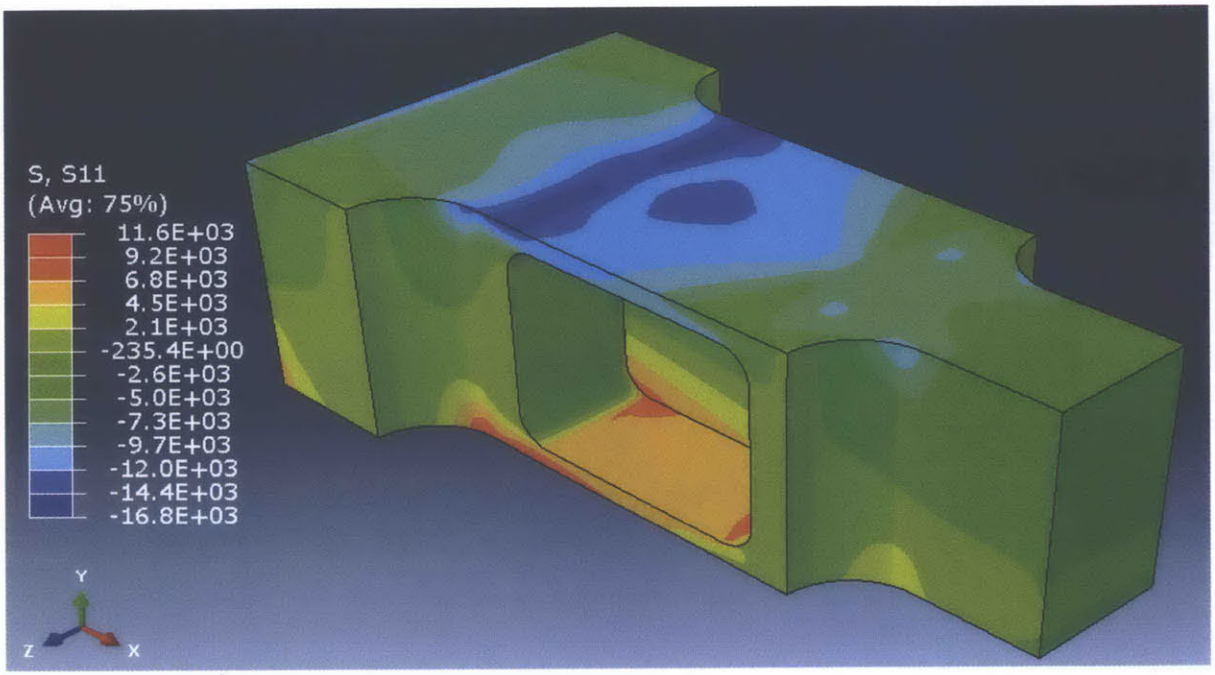

A summary of the stress analysis for the indenter columns considered is provided in Table 2.4. For this table, A is the cross-sectional area, I is the second moment of inertia about the bending axis, σ_{nom} is the nominal or reference stress calculated from the sectional properties A and I, σ_{max} is the peak stress obtained from the elastic FEA, and $k = \sigma_{max}/\sigma_{nom}$ is the stress concentration factor, as defined in Peterson's Stress Concentration Factors [15]. The factor of safety is with respect to the minimum yield strength of the indenter column, which is 40,000 psi for 6061-T6 aluminum. The significant stress concentration factors obtained for the rectangular solution roughly agree with simpler analytical solutions for a thin beam with a central hole loaded in bending [15]. Based on these results, it was decided to utilize the I-beam design with the 1/32 in. pocket radius. The smaller radius has a slightly lower factor of safety, however, it is still sufficiently high and provides a larger reduced cross-section for placement of the strain gage (0.1875 in. long v. 0.125 in. long).

Table 2.4: Results of stress analysis for indenter column

Shape	A (in.^{2})	I (in.^{4})	σ_{nom} (psi)	Pocket radius (in.)	σ_{max} (psi)	k	Factor of Safety
Rectangle	0.0150	0.000182	12443	0.03125	54500	4.38	0.73
				0.0625	39200	3.15	1.02
I-beam	0.0163	0.000137	15532	0.03125	16800	1.08	2.38
				0.0625	15500	1.00	2.58

2.3.3 Construction of Second Prototype

The second prototype was constructed based on the guidelines discussed above to improve the practicality and ease-of-use for the scratch testing device. This includes the hosting of the instrumentation to measure inputs of the dimensionless functions as well as the stress analysis of the indenter column geometry. The scratch testing device was designed to accommodate the skates as close to the scratch profile as possible to maintain a constant depth, which is why the column has a decreasing width towards its bottom. The device would be connected to the loading assembly through a self-aligning rod manufactured by Omega Engineering, which would allow for correction of slope for a test sample. The second prototype connected with the remaining support assembly utilized for the first prototype is shown in Figure 2.13.

Figure 2.13: Second prototype connected to loading assembly and support structure

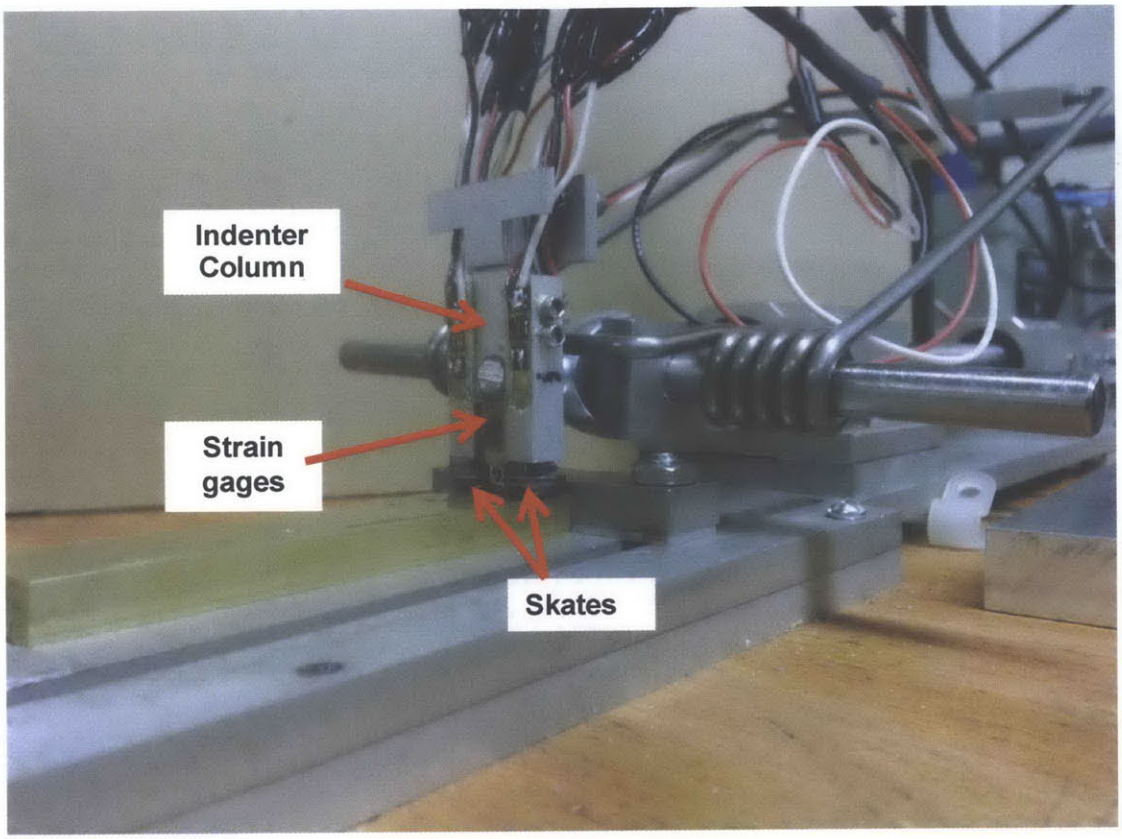

2.3.4 Strain Gage Calibration

Finite Element Analysis showed that the stress-strain distribution near the strain gage location was modified due to stress-risers from changes in geometry and relative stiffness along the length of the column. In addition, the exact dimensions of the column after machining are difficult to precisely measure to determine the actual cross-sectional properties. For this reason, strain gage data will be obtained in ideal loading conditions that will be used to establish empirical correlations for both normal load and frictional force at the indenter tip. This data may be extrapolated to differentiate and extract the normal load on the indenter during experiments.

As discussed, normal loads apply an axial stress and bending moment due to the offset position of the indenter tip with respect to the neutral axis position. Therefore, calibration of the scratch test device requires that the load be applied with the same offset. A testing rig was developed which would support the indenter column at its top while a C-shaped beam was attached to the bottom through a pin connection. The pin connection allowed the load attachment point to

swing freely and ensure a normal load application. The load application was through a threaded hook which was positioned at the centerline of the indenter offset, ensuring that the calibration loading configuration was identical to the service loading configuration for normal loads. The testing setup for normal loads is shown in Figure 2.14. Dead weights were applied for loading configurations of 10, 15, 25, 30, 35, and 40 lbs and strain measurements were recorded for all 4 strain gages. The two strain readings for the front and back faces of the indenter column were averaged for each loading configuration, and plotted against the applied load as shown in Figure 2.15. A linear regression with a zero intercept was fit to the data to allow for experimental data to be extrapolated for loading conditions outside of those investigated. The R-squared statistic for both of these linear regressions is better than 0.99, indicating a high degree of linearity. The calibration of the strain gages for normal load was performed with a tensile force when experiments will consist of compressive forces. However, for linear elastic isotropic materials such as aluminum, the difference between the tensile and compressive response will be minimal.

Figure 2.14: Testing setup for calibrating strain gages for normal loads

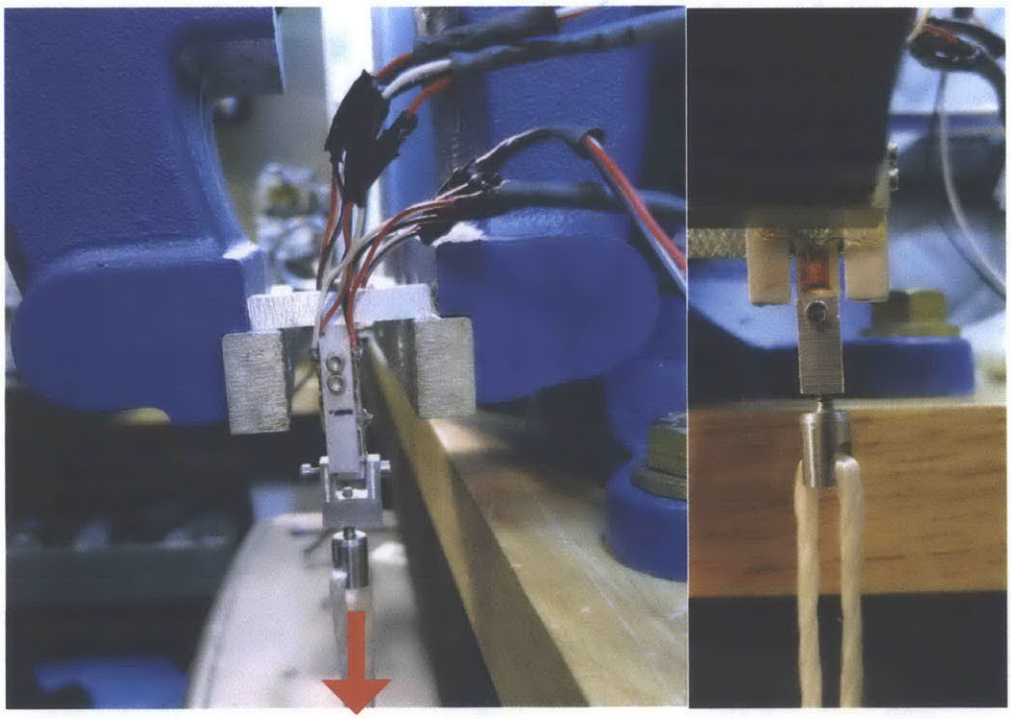

Figure 2.15: Strain gage calibration for normal loads

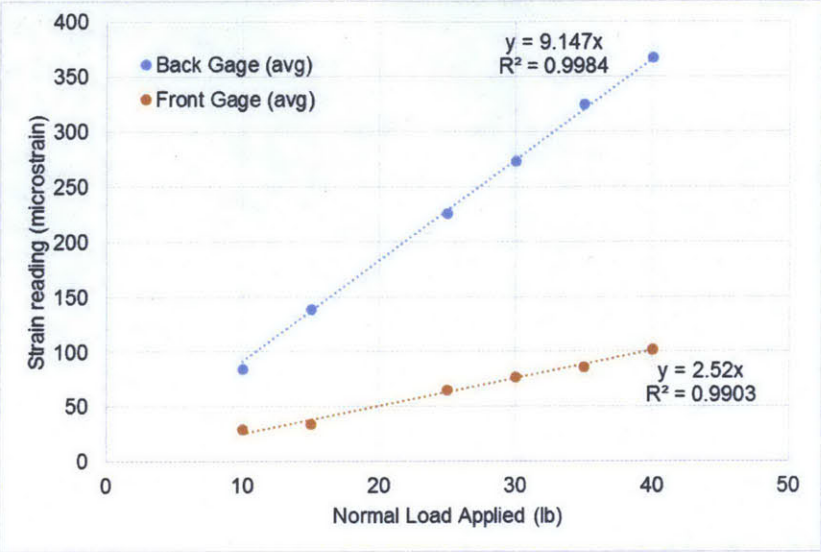

Pure bending moments were applied through a modified testing setup as shown in Figure 2.16. The method of attachment through the top of the indenter column was not a rigid connection, and therefore the device was able to slightly rotate out of alignment when loaded. The load was applied to the device through a screw and nut that was bearing on the top surface of the indenter column. The device was loaded with lower weight configurations because of the lever action at the flexible support, which caused significant stress in the supporting screws. The maximum weight considered was 15 lbs to ensure that the screws did not break, potentially damaging the device. Using the same method as the normal load calibration, the left and right gage measurements on the front and back face of the indenter column were averaged and plotted against the lateral load applied in Figure 2.17. A linear regression of the data points was performed, and the results again show a very high R-squared value indicating a highly linear behavior. However, for a pure bending moment it is expected that the tensile and compressive strain readings will be the same for the front and back face of the indenter column. We suspect that the discrepancy of the slope of the tensile and compressive readings is due to the rotation of the device during loading due to the flexible support connection. This rotation may allow for a non-uniform moment being applied through the threaded screw and nut attachment. To confirm this assumption, the device was flipped so that the back gages would be loaded in tension, and the front gages would be loaded in compression from the bending moment. Strain readings on the back gages in tension are within 2% of those obtained for the front gages in tension.

Therefore, we will assume that this slope is the same for both gages for pure bending loads like those generated from frictional forces at the indenter tip.

Figure 2.16: Testing setup for calibrating strain gages for bending loads

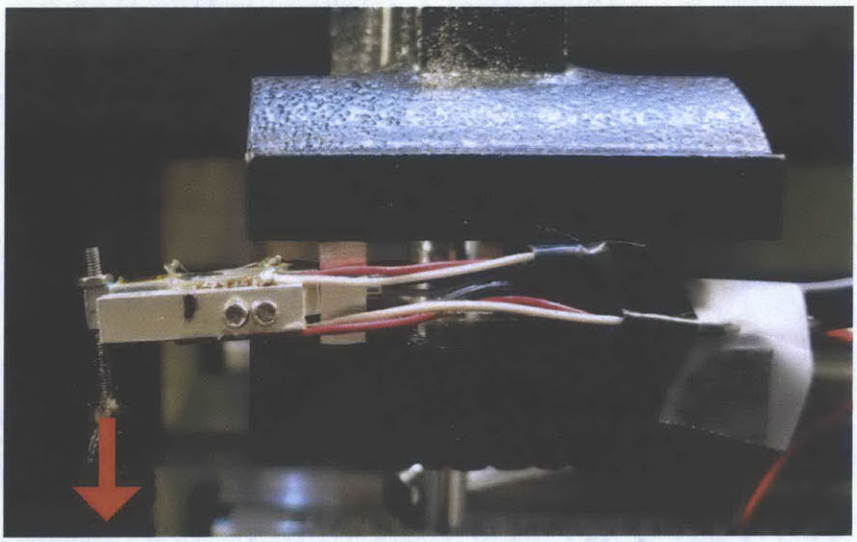

Figure 2.17: Strain gage calibration for bending loads

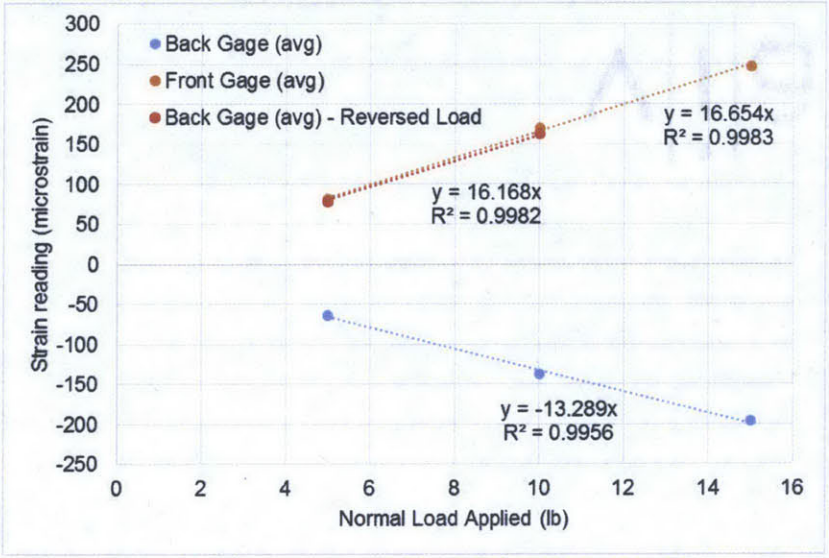

Chapter 2 – References

[1]. D. Tabor, The hardness of metals. Oxford University Press; 1951.

[2]. K.-J. Bathe, Finite Element Procedures, Printice Hall, Pearson Education, In., 2006.

[3]. ASM International, Atlas of Stress Strain Curves, 2002.

[4]. P.E. Labossiere, "Chapter 5: Mechanical Properties and Performance of Materials," *ME354 Mechanics of Materials Laboratory at U. Washington*, 2007.

[5]. ASM International, "Roll Forming of Axially Symmetric Components," *ASM Handbook Vol. 14*, 2005.

[6]. M. Dao, N. Chollacoop, K.J. Van Vliet, T.A. Venkatesh, S. Suresh, "Computational modeling of the forward and reverse problems in instrumented sharp indentation," *Acta Materialia,* vol. 49, pp. 3899-918, 2001.

[7]. Century Spring, "Material Properties," pp. 377-381, 2014.

[8]. R.G. Budynas and J.K. Nisbett, Shigley's Mechanical Engineering Design, *Ninth Edition*, McGraw-Hill College, 2010.

[9]. S.C. Bellemare, M. Dao, S. Suresh, "Effects of mechanical properties and surface friction on elasto-plastic sliding contact," *Mechanics of Materials,* vol. 40, pp. 206-19, 2008.

[10]. Hirox, KH-8700 Digital Microscope User Manual, 2013.

[11]. Omega Engineering, "Practical Strain Gage Measurements," *Application Note 290*-1, pp. E-94-130, 1999.

[12]. Vishay Precision Group, "Strain Gages and Instruments: Strain gage selection: criteria, procedures, recommendations," *Tech Note TN-505-4 Rev. 3*, pp. 49-64, 2010.

[13]. Dassault Systemes, "Abaqus Analysis User's Manual," 2012.

[14]. ASM Interational, "Properties and Selection: Nonferrous Alloys and Special-Purpose Materials," *ASM Handbook Volume 2*, 1990.

[15]. W.D. Pilkey and D.F. Pilkey, Peterson's Stress Concentration Factors, *Third Edition*, John Wiley & Sons, 2008.

Chapter 3: Applications of Scratch Testing Device

This chapter details implementation of the scratch testing device and instrumented scratch testing methodology. A novel application is highlighted where a scratch test through a welded connection is performed and the evolution of mechanical properties is observed. The incorporation of LVDT instrumentation to obtain scratch measurements of a brass material is also described. Finally, recommendations for future prototypes are provided.

3.1 Application: Scratch through a Welded Connection

The instrumented scratch testing method allows for the local measurement of the yield strength and strain hardening exponent as the indenter ploughs a scratch through the sample material. In this section, we detail a scratch through a butt-welded connection to illustrate the testing device and method's ability to monitor the evolution of mechanical properties along the length of a scratch. To date, the existing literature related to scratch testing has been limited to wear applications or scratches through homogeneous materials. This application presents a powerful condition assessment and quality control technique for practicing engineers.

Welding is a joining technique that is used on structures and assemblies in many industries to rigidly connect metallic components. During welding, the base metal near the heat source is subjected to significant thermal stress resulting in a heat-effected zone (HAZ) where the rapid heating and cooling causes changes in the strength and ductility of the material. The scratch testing device and testing method allow for the quantification of changes in mechanical properties from the unaffected base metal, through the HAZ, and into the filler weld metal.

We created a butt-welded connection using two quarter inch thick plates of 4130 low-alloy high strength structural steel. The plates were beveled and welded with an E70 filler metal in accordance with American Welding Society (AWS) and American Institute of Steel Construction (AISC) guidelines by a certified welder. The surface was milled to ensure that the base-metal and filler metal were planar so that the testing device could make a scratch through the welded connection. Prior to testing, the surface was polished with up to 440 grit SiC paper and lubricated. The butt-welded test sample is shown in Figure 3.1 Preliminary tests on the steel material showed that chipping was occurring along the length of the scratch, preventing the measurement of scratch profile parameters. Chipping occurs because the frictional forces generated between the tungsten carbide indenter tip and steel sample are too high. To

eliminate the occurrence of chipping, the testing sample was elevated such that the scratch was performed at a lower attack angle. This has the same effect of increasing the included angle of the indenter tip, and will reduce the accuracy of the predictive equations for ductile properties because the angle no longer matches the conditions utilized by Bellemare et al. However, this step was necessary for measurements in the steel, and the observed changes in material during the scratch test is still of significant value.

Figure 3.1: Photo of butt-welded connection and milled surface after polishing

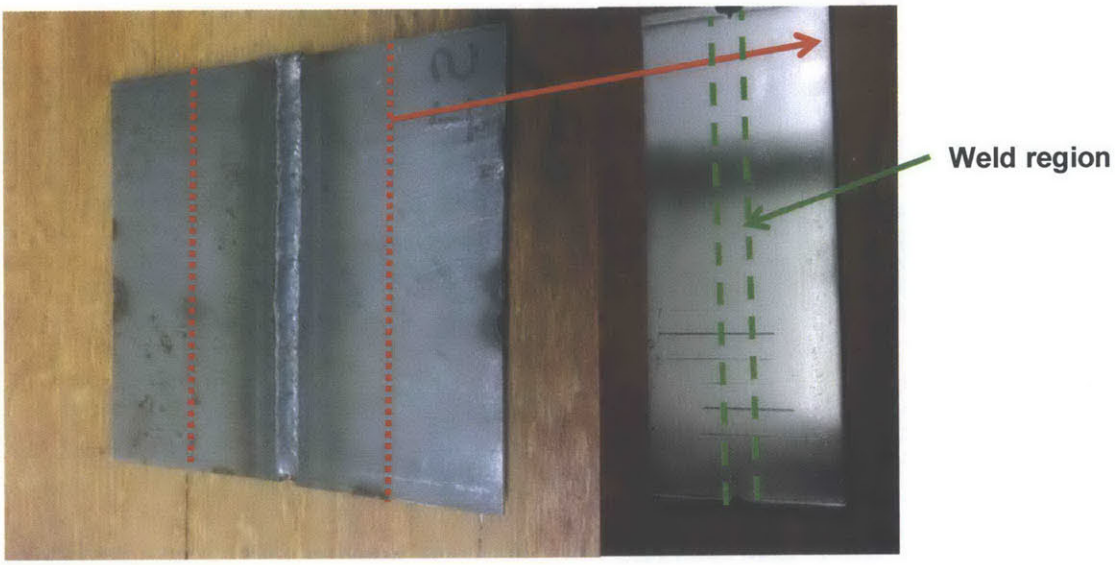

Scratch tests were conducted at a velocity of approximated 1.58 mm/second for a total length of approximately 35 mm (1.375 in.). The strain gage signal in microstrain is shown over the duration of the experiment in Figure 3.2 for the back left (BL), back right (BR), front left (FL) and front right (FR) gages. The back gages experience a greater absolute strain magnitude because of the off-centered position of the indenter with respect to the neutral axis of the indenter column. The front and back gage readings were averaged over time, and the gross strain was determined (back gage average + front gage average = gross strain). This is appropriate given the consistent linear behavior of both the front and back gages to bending moments from frictional forces as shown in Figure 2.17. With the bending moment from friction removed, the normal reaction force was obtained using the best fit equations shown in Figure 2.15. The reaction force along the length of the scratch is shown in Figure 3.3. There is a clear distinction between the base metal, HAZ, and filler weld metal. As expected, the HAZ which has been plastically deformed by thermal stresses during weld fabrication shows a gradient in

hardness with the sharpest peak adjacent to the weld metal. In addition, the E70 filler weld metal has a higher hardness than the original 4130 steel base metal. This data also allows for measurements of the relative size of the HAZ. Based on Figure 3.3, the relative width of the heat affected zone is approximately 0.08 in. (2 mm). The HAZ would be more clearly defined had the test been performed at a lower velocity, reducing the length of the transient period that occurs when mechanical properties change.

Figure 3.2: Raw data signal from strain gages during weld experiment

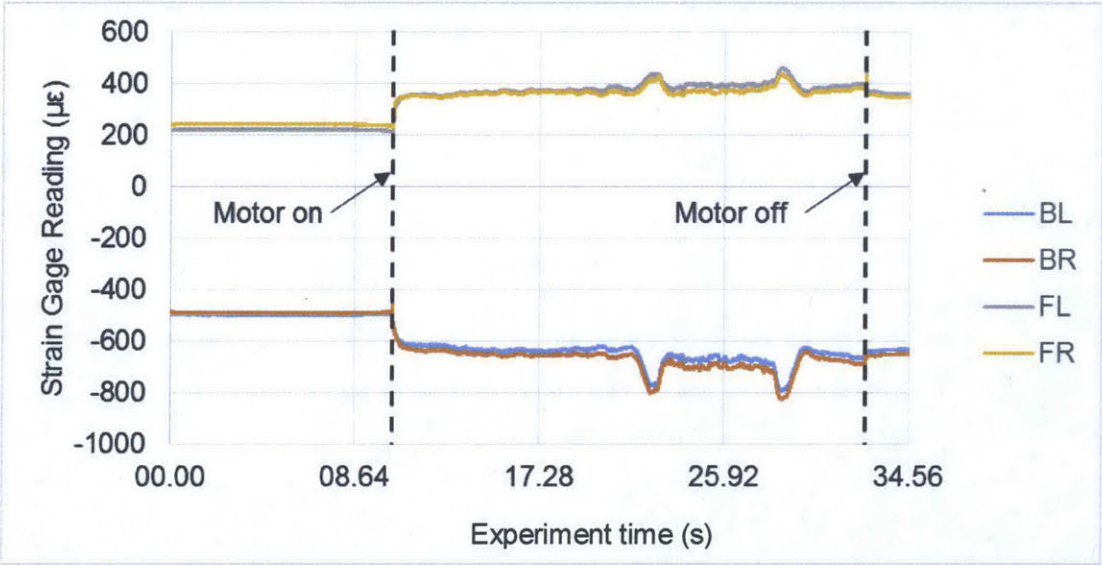

Figure 3.3: Calculated reaction force clearly indicating transitions in material properties

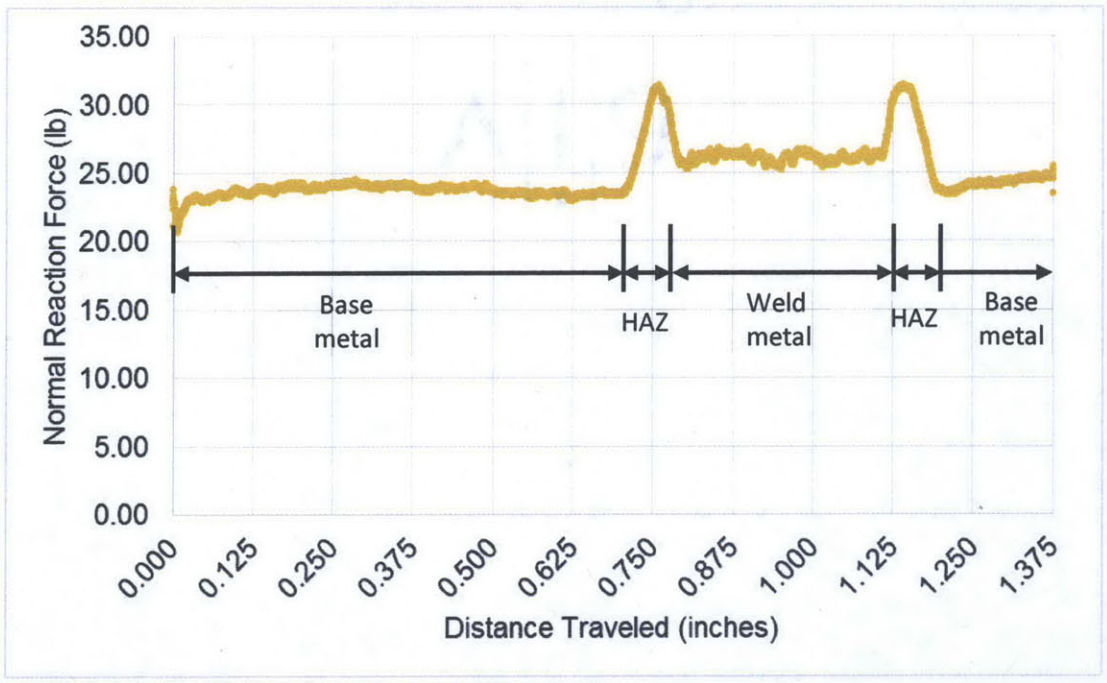

We imaged the resulting scratch profiles with a Hirox digital microscope to evaluate the change in scratch profile dimensions along the length of the scratch. The results are shown in Table 3.1 below. The averaged pile-up ratios for the base metal, HAZ, and weld are 0.63, 0.68 and 0.66, respectively. The increase in pile-up ratio from the base metal to the HAZ is indicative of a decrease in the strain hardening exponent due to work hardening of the material. The results also show that the depth of scratch changes moderately during the scratch experiment. Examining the depth of gouging at the contact points of the skates and sample indicated that the depth of penetration noticeably decreased when the indenter was ploughing through the harder materials. This is attributed to the change in reaction force at the indenter tip when the scratch progresses through a harder material, such as the HAZ of the weld. Since the applied load is constant, the increase in the reaction force at the indenter tip causes a corresponding decrease in the residual load applied to the skates. One possible solution is to increase the radius of the skates, such that the applied load is distributed over a greater area, and there is less gouging of the sample material away from the scratch indenter for any applied load. Therefore, when the reaction force at the indenter increases, the effect on the depth of the skates will be minimized, and a constant depth through various materials will be achieved.

Table 3.1: Scratch profiles measured with digital microscope

Profile #	Base Metal		HAZ		Weld	
	h_d (μm)	h_p (μm)	h_d (μm)	h_p (μm)	h_d (μm)	h_p (μm)
1	26.3	15.6	25.3	16.2	23.6	16.2
2	26.5	17.4	25.3	17.9	24.9	15.4
3	26.7	16.7	25.8	17.7	24.3	15.2
4	26.6	17.3	25.0	16.9	23.9	16.1
5	26.0	16.7	24.0	17.2	23.5	16.4
Average	26.4	16.7	25.1	17.2	24.1	15.9
Stdev	0.3	0.7	0.7	0.7	0.6	0.5

Although we were able to obtain the necessary inputs for the dimensionless functions determined by Bellemare et al., we were unable to accurately estimate the yield strength and strain hardening exponent of the base metal, HAZ, and weld metal. Discrepancies in the mechanical properties predicted by dimensionless functions are discussed in the following sections. Despite the current accuracy limitations, this experiment highlights a novel ability of the scratch testing method to monitor the evolution of mechanical properties in areas where prior plasticity or damage has occurred. These are of great concern to practicing engineers during life assessment, as well as new manufacturing. The scratch testing device and method could be utilized as a tool for ensuring that welded connections are fabricated within safe operating limits by monitoring changes in the HAZ.

3.2 Continuous Scratch Profile Measurements

The second prototype was designed to incorporate an LVDT device to measure the remaining scratch parameters by contacting the pile-up during a scratch experiment. The LVDT was attached to the top of the prototype such that no loads from the indenter column would be applied to the instrumentation. Two screws were used to apply a compressive clamping force and hold the LVDT. This method allowed for the elevation and orientation of the LVDT to be easily modified during an experiment. The normal contact tip for the LVDT was replaced with a contact wedge assembly. The wedge is 4140 hardened steel with a rounded single cylindrical

curvature tip that is intended to be in contact with the scratch pile-up material during the test. The wedge has a through hole to accommodate a 0.020 in. diameter rod that is press fit into the hole. This rod rests inside two Teflon bearings, which were manufactured by drilling a 0.020 in. hole within a M2.5 Teflon screw acquired from Technique Engineering (Lake Forest, IL). These Teflon bearings were threaded into an aluminum C-shaped beam that allows the contact wedge to freely rotate so it will contact both sides of the scratch pile-up, and effectively average the height of each side during an experiment. The LVDT assembly connected to the scratch testing device is shown in Figure 3.4.

Figure 3.4: Scratch testing device with LVDT holder and contact wedge assembly

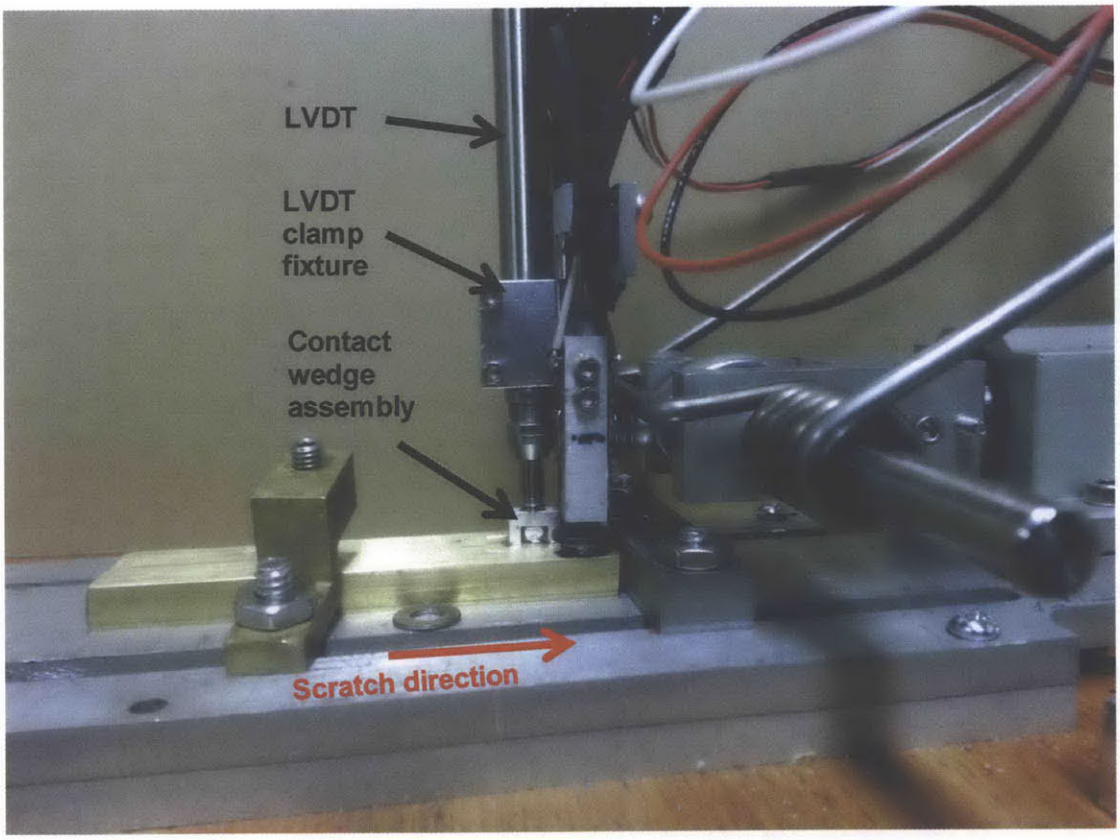

Scratch tests were performed on a soft brass material (360 or Naval brass) which would not chip even with the higher frictional forces for the tungsten carbide indenter tip. The normal reaction force on the indenter tip was calculated from the strain gage readings in the same method as Section 3.1. The LVDT produces a linear voltage signal that was calibrated with a steel washer which was measured with a micrometer to the nearest 0.0005 inches. The changes in voltage can be related to changes in height by making a linear interpolation between

the recorded voltage and the associated linear displacement. The calculated reaction force from strain gages and the calculated pile-up height from the LVDT signal are shown in Figure 3.5. The plot shows that while the reaction force quickly reaches a steady state value, the LVDT takes almost 20 seconds (20 mm of scratch length) to reach a steady state. Experiments showed that lower scratch velocities improved the LVDT signal, and the use of a motor with a higher gear reduction, and therefore lower linear velocity, would improve the application. The experiment shows that the average pile-up measured during steady state is approximately 19 microns, and the average reaction force on the indenter column is approximately 30.4 lb.

Figure 3.5: Calculated load and measured pile-up for a scratch experiment with brass

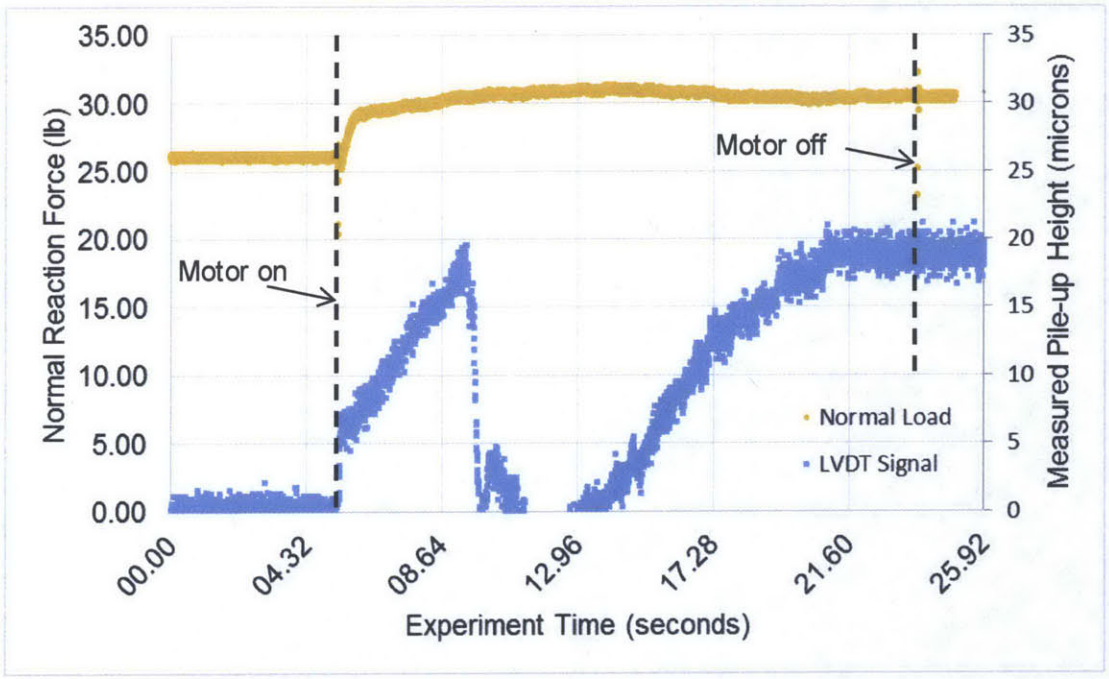

The pile-up height obtained from the LVDT was compared to measurements of a scratch using digital microscopy. The resulting scratch profile is shown in Figure 3.6, and has an average measured pile-up height of 23.3 microns, and a scratch depth of 35.5 microns. Therefore, the compressive force of the LVDT spring and mass of the LVDT plunger and contact wedge assembly compresses the pile-up by approximately 4 microns. This effect would be reduced by using an LVDT with a smaller spring constant. Using these height measurements, the theoretical scratch radius should be equal to 164.2 microns. However, measurements of the scratch profile found a radius of 269.2 microns, an increase of almost 64%. The included angle of the residual scratch profile is around 155°, which is significantly larger than the 140.6° used in

the equations by Bellemare et al, and results in a much lower scratch hardness reading than would be expected. The significant increase in the scratch width can be attributed to lateral movement of the scratch tip during the experiment. The method of holding the indenter tip, a close-fit hole with a set screw, is not sufficiently rigid for the level of precision required.

Figure 3.6: Scratch profile through brass obtained with digital microscopy

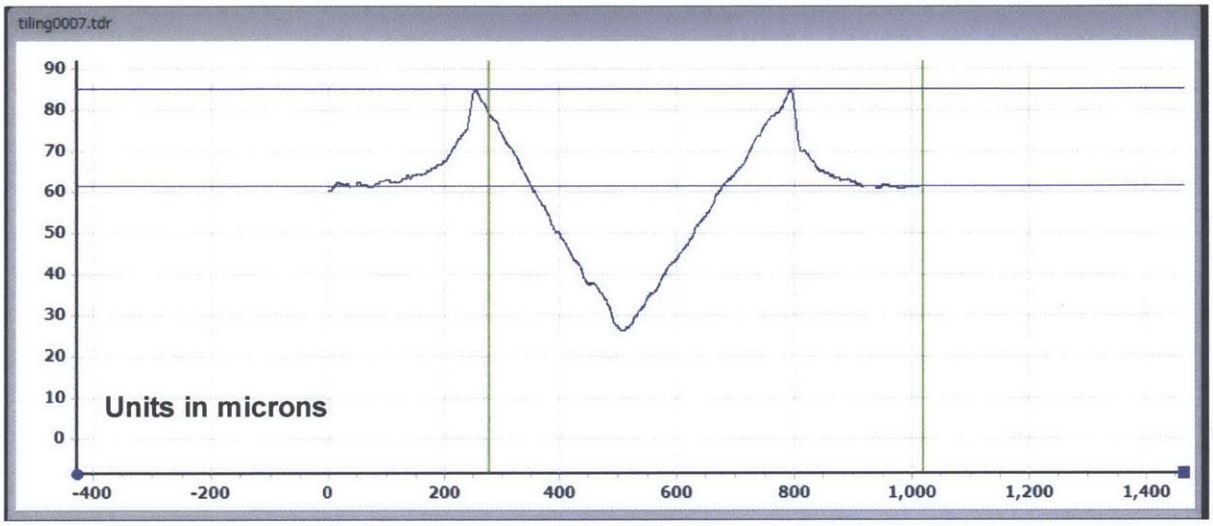

3.3 Recommendations for Future Prototypes

This project has allowed for the design and development of two prototype scratch testing devices. The second prototype improved on the original design by incorporating instrumentation, reducing the overall size, and utilizing an efficient and well-designed indenter column for maximizing axial strain resolution. Recommendations for future designs are as follows:

- The accuracy of the second prototype was reduced by the relative flexibility of the indenter tip within the indenter column. The indenter tip was held with a close-fit hole and small set screw, which was not sufficient to prevent lateral movement of the tip by several microns. The result is that the scratch experiments performed using the second prototype create a residual scratch which no longer matches the ideal conical shape of the indenter. This largely explains the discrepancy in predicted material properties when compared to tensile testing of the steel base metal and brass. Because the indenter was able to move, the actual area resisting load was greater than intended, reducing the

calculated hardness values and changing the shape of material pile-up. The dimensionless functions derived by Bellemare et al. are specific to a conical indenter with a 140.6° included angle, and the greater the experiment deviates from this geometry the less accurate the method will be. Future designs should consider a press-fit or threaded connection.

- The tungsten carbide material used for the indenter tip generates significant friction during scratch experiments. The dry coefficient of friction for the tungsten carbide on steel is more than 2.4 times greater than the friction coefficient reported by Bellemare et al. for a diamond tipped indenter. The result is that frequently during scratch experiments chipping was preventing the measurement of ductile properties, especially for materials with low strain hardening values such as aluminum. Tungsten carbide was selected because a diamond indenter matching our geometry and length-scales was not commercially available. Future designs should make great efforts to obtain diamond indenters, or increase the included angle of the indenter. Increasing the included angle of the indenter was shown to resolve the chipping problem during scratches performed on high strength steel. However, increasing the included angle of the indenter will result in less plasticity of the material as well as the need for reevaluation of the dimensionless scratch functions.
- The double torsional spring is an effective method of applying significant load with a compact design. However, the desired rotational preload is difficult to obtain with a longer moment arm. The relatively small sectional dimensions of the spring coil lead to significant deflection of the loading arms which is not transferred to the torsional coils. Reducing the length of the preload arm will reduce this effect. The rotation at the base of the torsional spring can be calculated using a simple cantilever beam approximation.
- During a scratch experiment, the skates should be aligned such that the indenter ploughs an even scratch through the material, so that the resulting pile-up height on either side of the scratch is approximately equal. With the existing design, this method requires tedious iterations to adjust the elevation of the skates, perform the scratch, image the scratch, and make appropriate corrections. In addition, the only method of ensuring that the both skates are making solid contact with the test sample is to apply more load than needed so that the skates produce a clear gouge in the material. Adding additional load to the skates reduces the load applied to the indenter column to achieve

greater penetration depths in the sample material, and requires that the depth of penetration be reduced. A contact indicator or strain gage attached to the skates could be used as an aid for ensuring a level device and uniform contact pressure applied at each skate. Also, increasing the radius of the skates will distribute the contact pressure over a greater area, and minimize the gouging of the sample material at the skate location. An extremely fine thread for the skates themselves would allow for more precise adjustment of their relative elevation.

- The linear actuator provides significant ploughing force with a relatively small design. However, a greater gear reduction will allow for even higher applied loads at lower velocities. The velocities that these tests were conducted at are more than 100 times greater than those performed with the commercial Nanotest equipment produced by Micro Materials. A lower test velocity will improve measurements, may reduce the distance required to reach steady state, and reduce possible dynamic effects.

- The existing design performs its intended function. However, for ease of use to the user additional consideration must be given to make the sensitive components more robust. The strain gages, terminal pads, and associated wiring should be better protected from accidental misuse and the environment. In addition, the strain gage wiring could be modified to a mechanical connection, so that the device could be more easily transported without worrying about damaging the critical instrumentation components.

- The LVDT assembly was an effective method of measuring the scratch pile-up height. However, the method took a significant amount of time to reach a steady state condition, which can be attributed to the relatively high load applied by the LVDT's linear spring (30+ grams) and velocity limitations of the linear actuator motor. Testing should be conducted at lower velocities to see if steady state can be achieved over a smaller scratch length. Our results indicate that another method of measurement may be desirable, although mechanical contact through the LVDT provided acceptable accuracy after applying a correction factor for local compaction of the scratch pileup.

- The indenter column, skates, torsional spring, LVDT assembly, and linear actuator may be readily incorporated into a portable testing system. While the second prototype successfully minimized the profile of the indenter column and skates, additional work is required to reduce the layout of the supporting structure. This support structure must

also be suitable for attachment to common structural assemblies, such as flanges or webs of I-beams, gusset plates, or cylindrical pressure vessels.

Conclusions

Instrumented scratch testing is an appealing alternative to existing non-destructive techniques such as hardness testing because it provides information about a material's mechanical properties including yield strength and ductility, similar to a destructive tensile test. In this thesis, I have provided a thorough background on both the historical and current research related to scratch testing methods. The review focused on trends observed during experiments and simulations including the effect of friction between the indenter tip and sample material. In addition, the advantages of instrumented scratch testing over alternative techniques such as instrumented normal indentation were discussed.

Two scratch testing prototypes and associated components were successfully designed and developed. This includes methods of load application, indenter column design, instrumentation and the support structure. The first prototype successfully validated the displacement control mechanism, a key innovation towards performing scratch tests outside of a laboratory environment, and reducing the number of variables that must be measured after an experiment. The second prototype greatly reduced the size of the device and incorporated instrumentation to measure the reaction force and residual scratch pile-up.

A novel application of the scratch testing device was highlighted by performing a scratch through a butt-welded connection. The scratch test was able to clearly identify changes in mechanical properties related to the base metal, heat-affected zone (HAZ), and weld metal. No other testing technique allows for the continuous measurement of local mechanical properties in this manner. This type of testing method can be utilized for condition assessment of existing structures as well as quality control in manufacturing. In addition to welded connections, local mechanical properties are desired by practicing engineers in any location where prior plastic deformation due to overload or wear has occurred.

The incorporation of the LVDT to measure the residual scratch pile-up was demonstrated with experiments on a soft brass material. The ability to measure the residual scratch pile-up, combined with the scratch depth that is fixed through the depth control mechanism and reaction force evaluated through strain gages, allows for the continuous measurement of all necessary inputs required to evaluate mechanical properties using the reverse algorithms developed by Bellemare et al.

The accuracy of the mechanical properties determined predicted through this device is low compared to the actual values obtained through traditional tensile testing. However, the reasons for these discrepancies are explained, and recommendations for future iterations of the scratch testing device are provided. This thesis provides a practical and technical foundation for developing a portable instrumented scratch testing device that is simple to implement and allows for innovative testing techniques to evaluate localized changes in mechanical properties.

APPENDIX A

Detail Drawings for Key Components

35 LB LOAD
NO SET SCREW
COUNTERSUNK BEARING SCREW

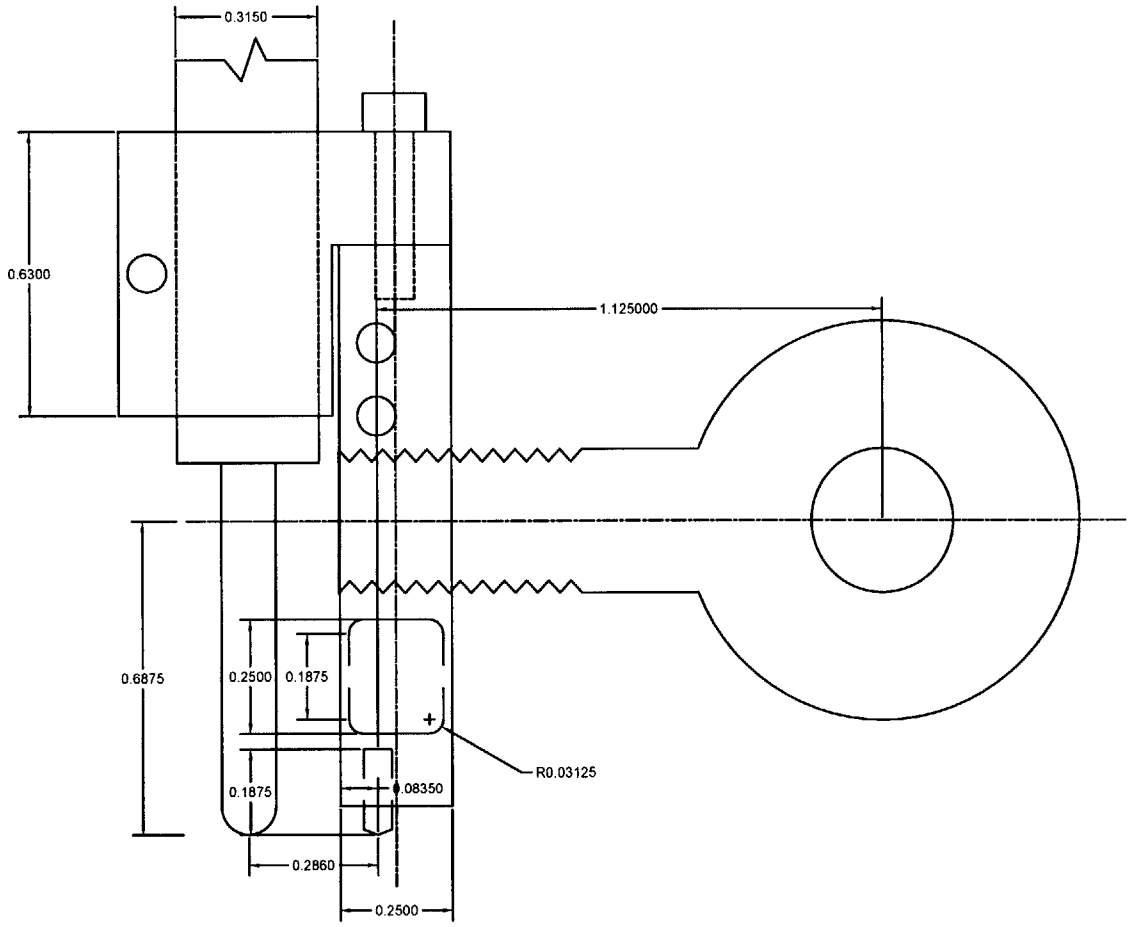

PRODUCED BY AN AUTODESK EDUCATIONAL PRODUCT

PRODUCED BY AN AUTODESK EDUCATIONAL PRODUCT

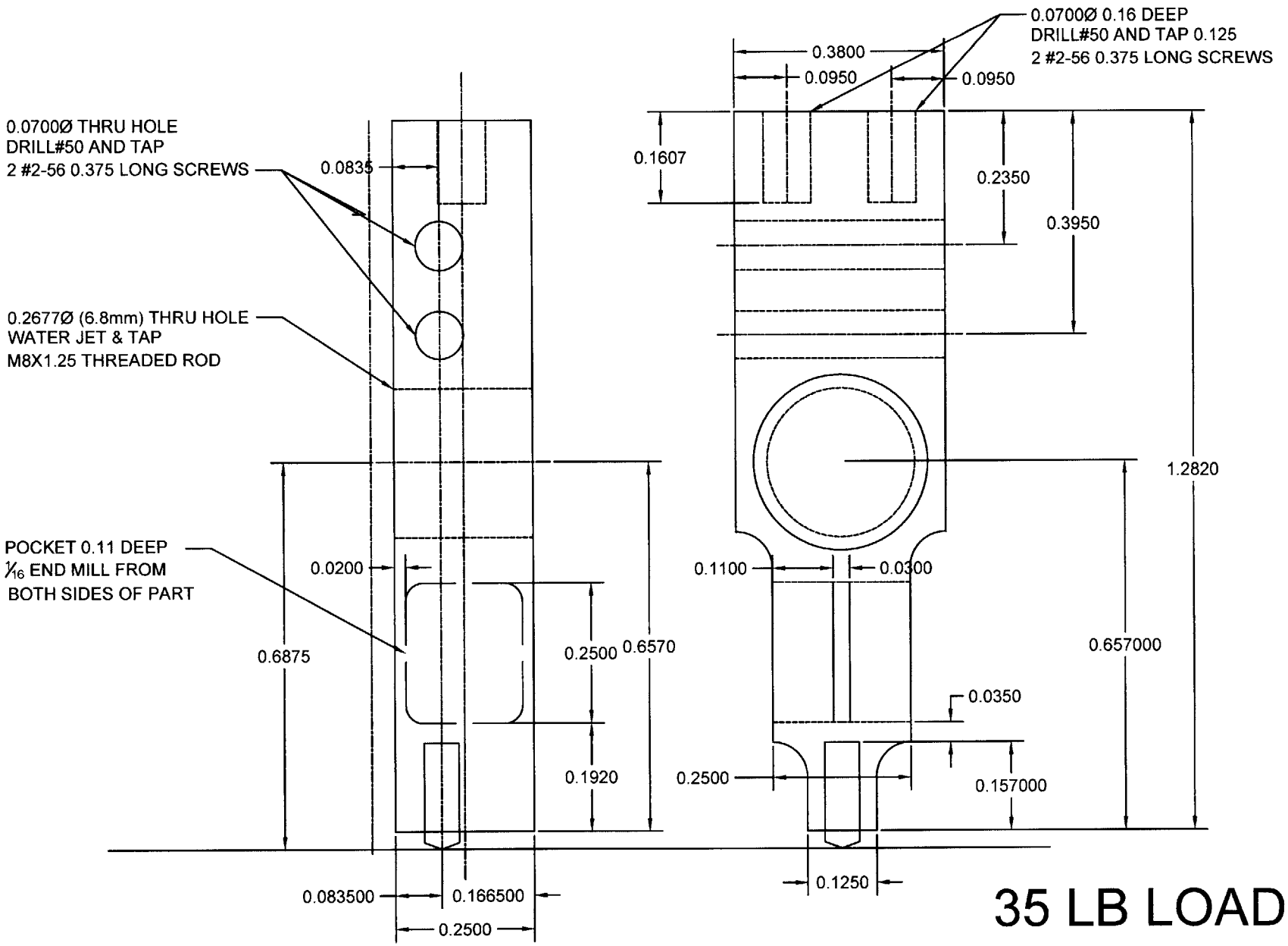

35 LB LOAD
COLUMN
QUANTITY =

PRODUCED BY AN AUTODESK EDUCATIONAL PRODUCT

PRODUCED BY AN AUTODESK EDUCATIONAL PRODUCT

35 LB LOAD
COLUMN-LEG
QUANTITY = 2

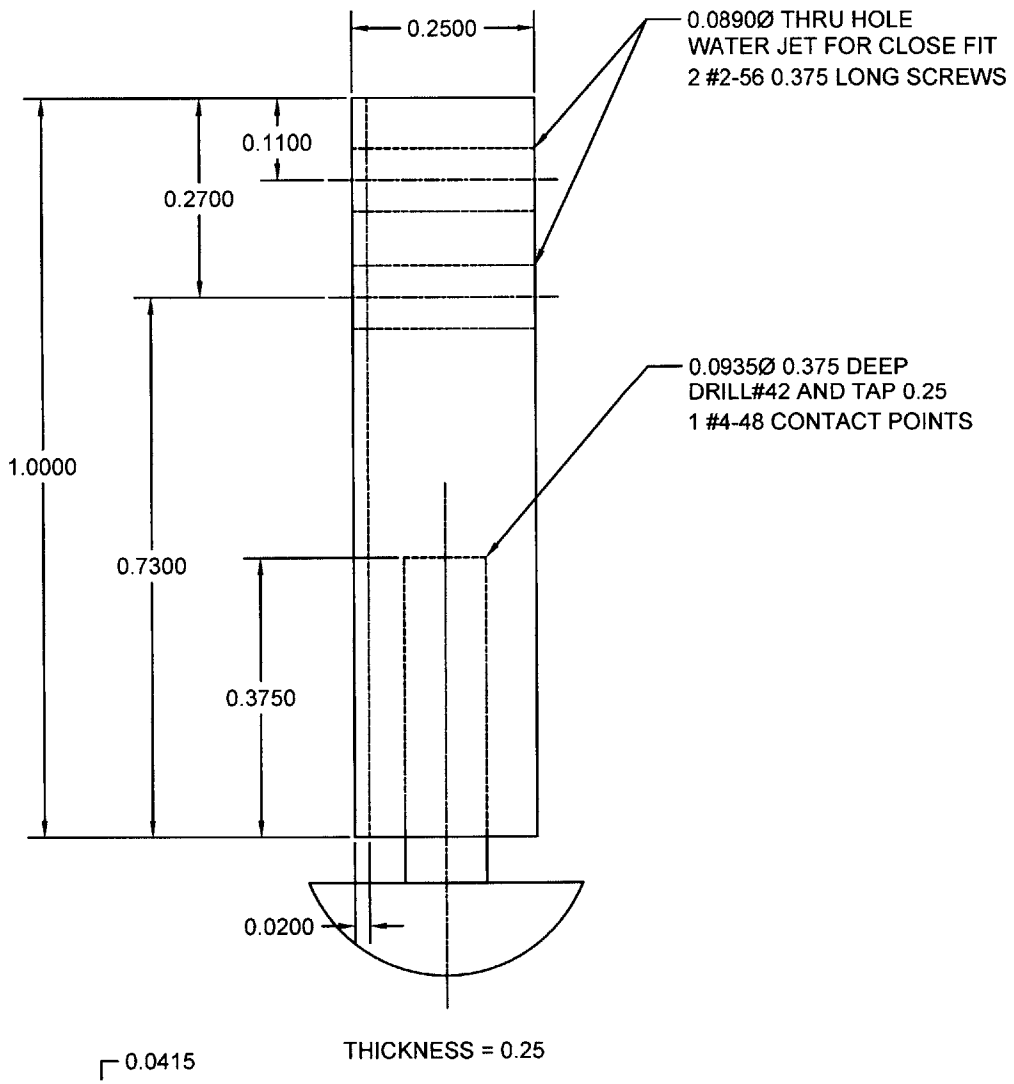

PRODUCED BY AN AUTODESK EDUCATIONAL PRODUCT

PRODUCED BY AN AUTODESK EDUCATIONAL PRODUCT

DIMENSIONS IN INCHES

LVDT ADAPTER
QUANTITY = 1

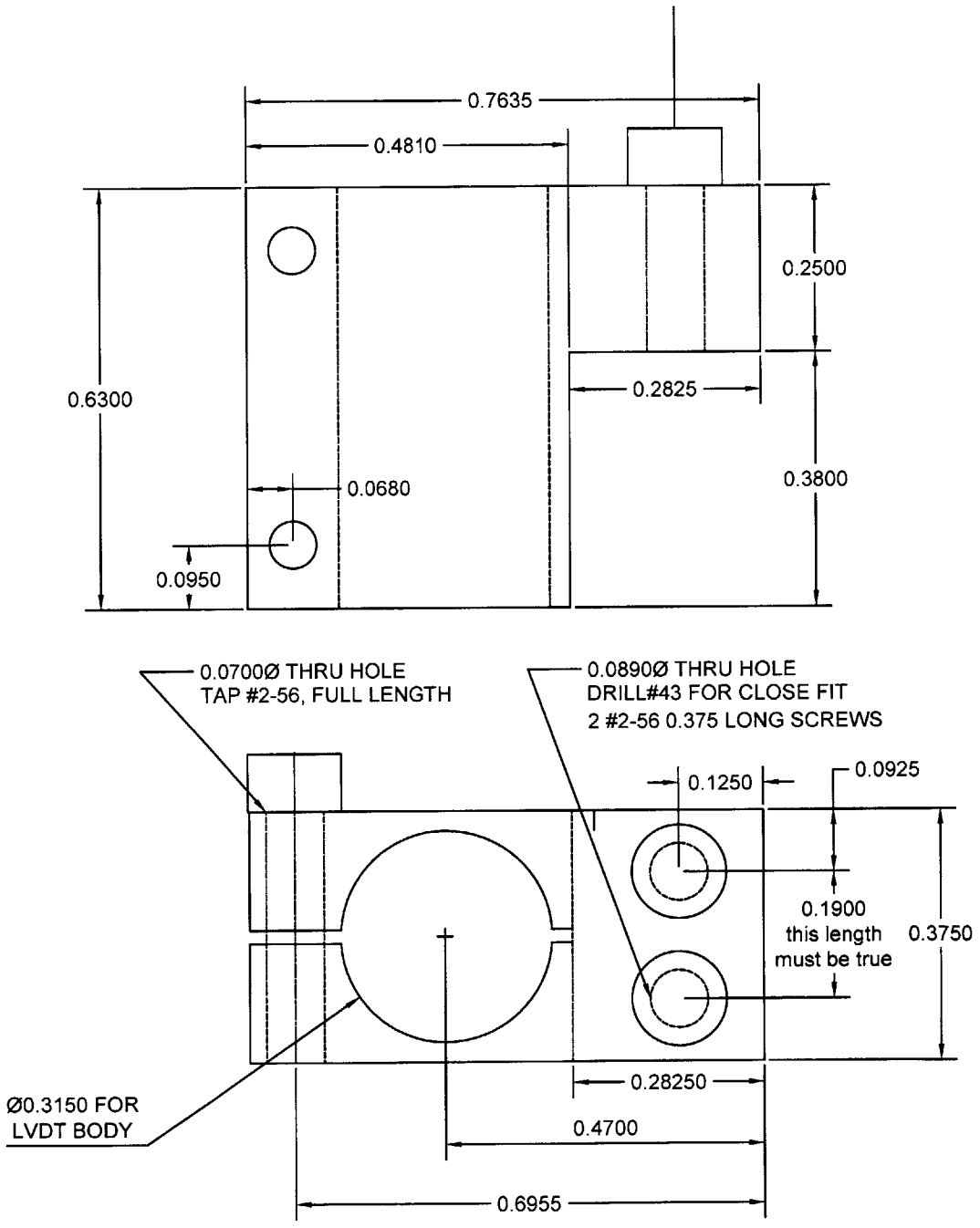

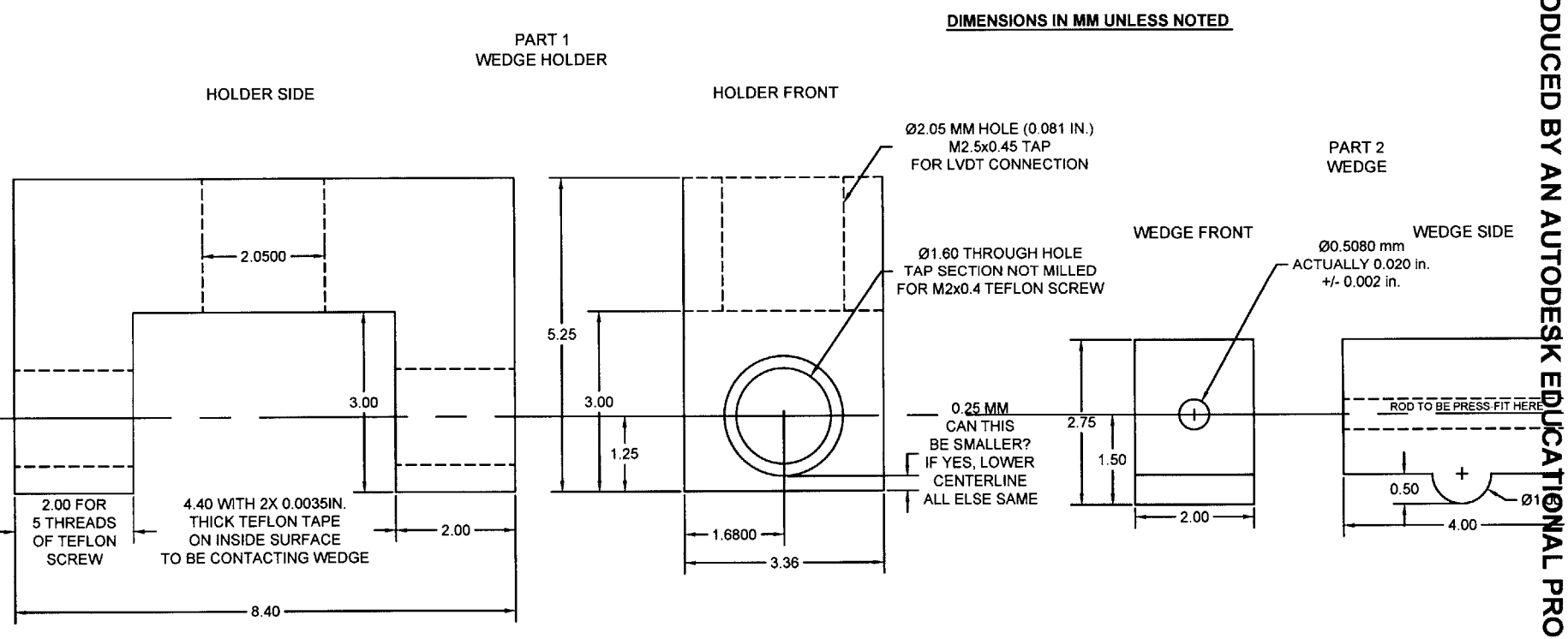

WIRE CLAMP

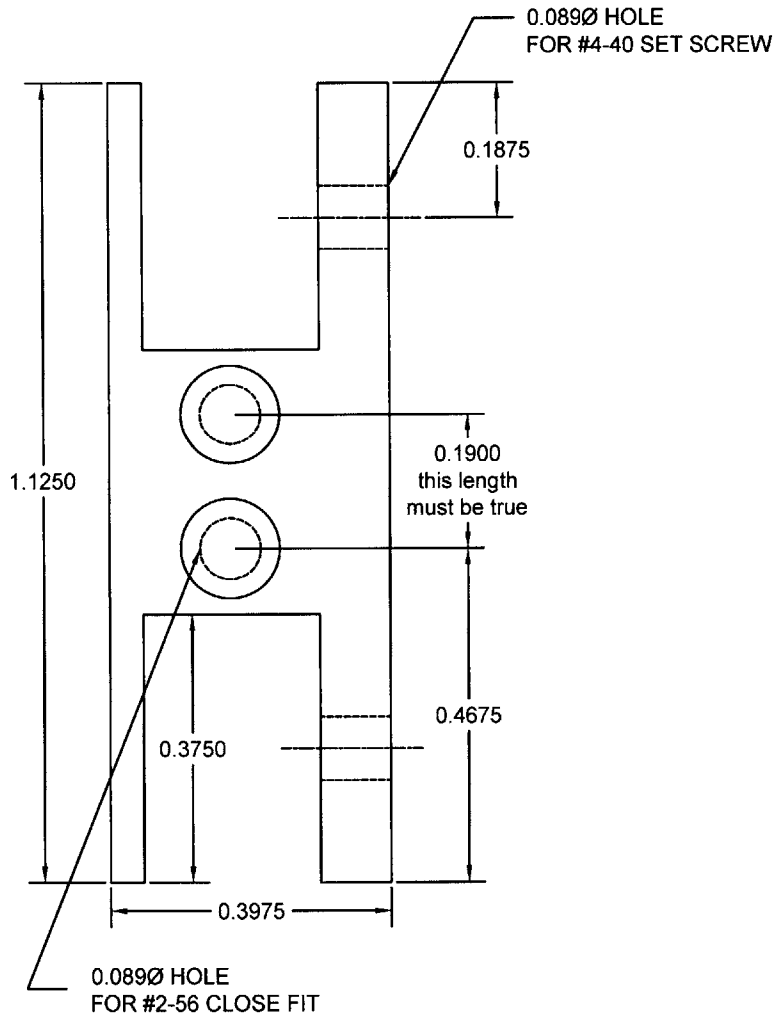

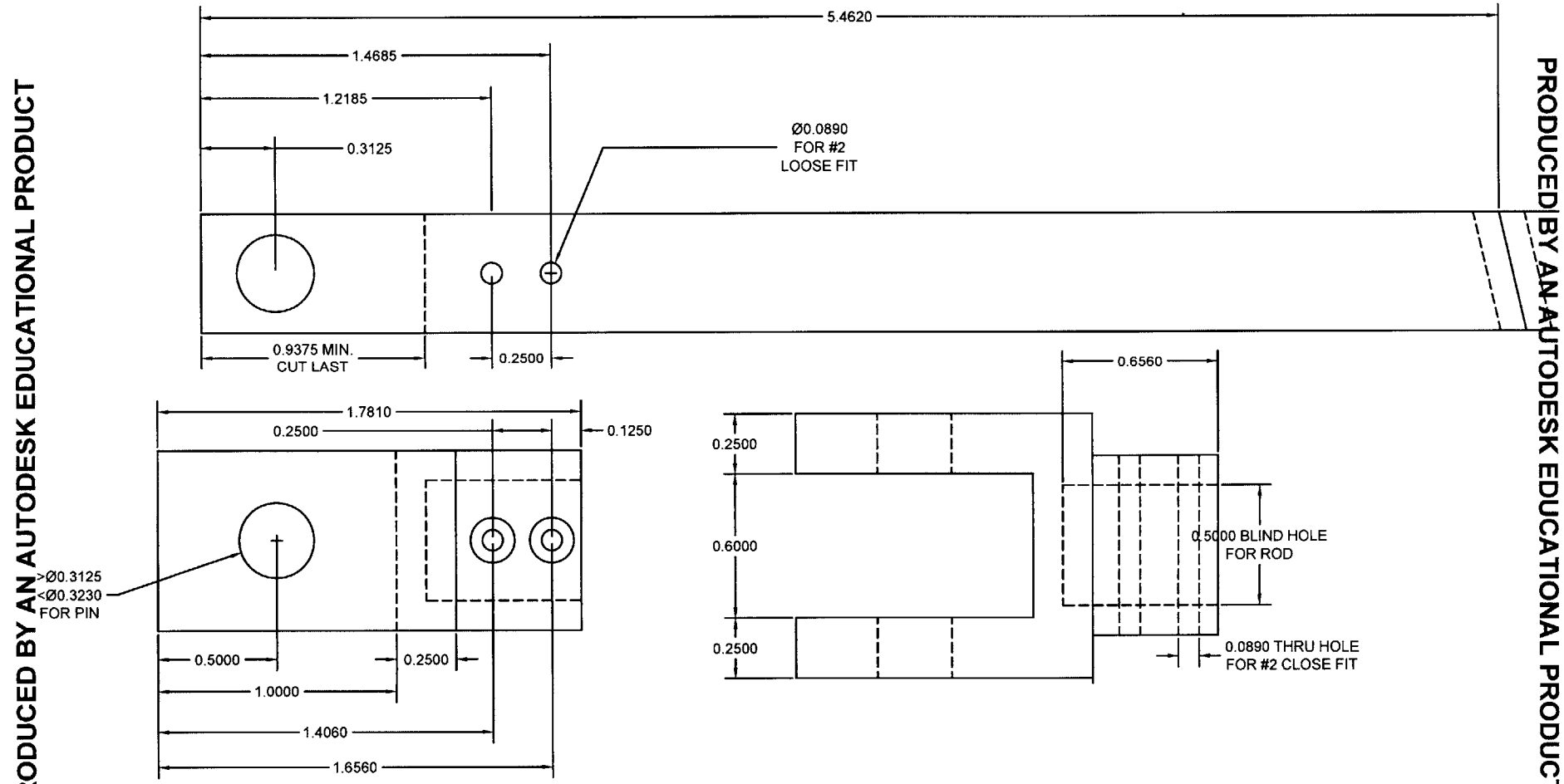

PRODUCED BY AN AUTODESK EDUCATIONAL PRODUCT

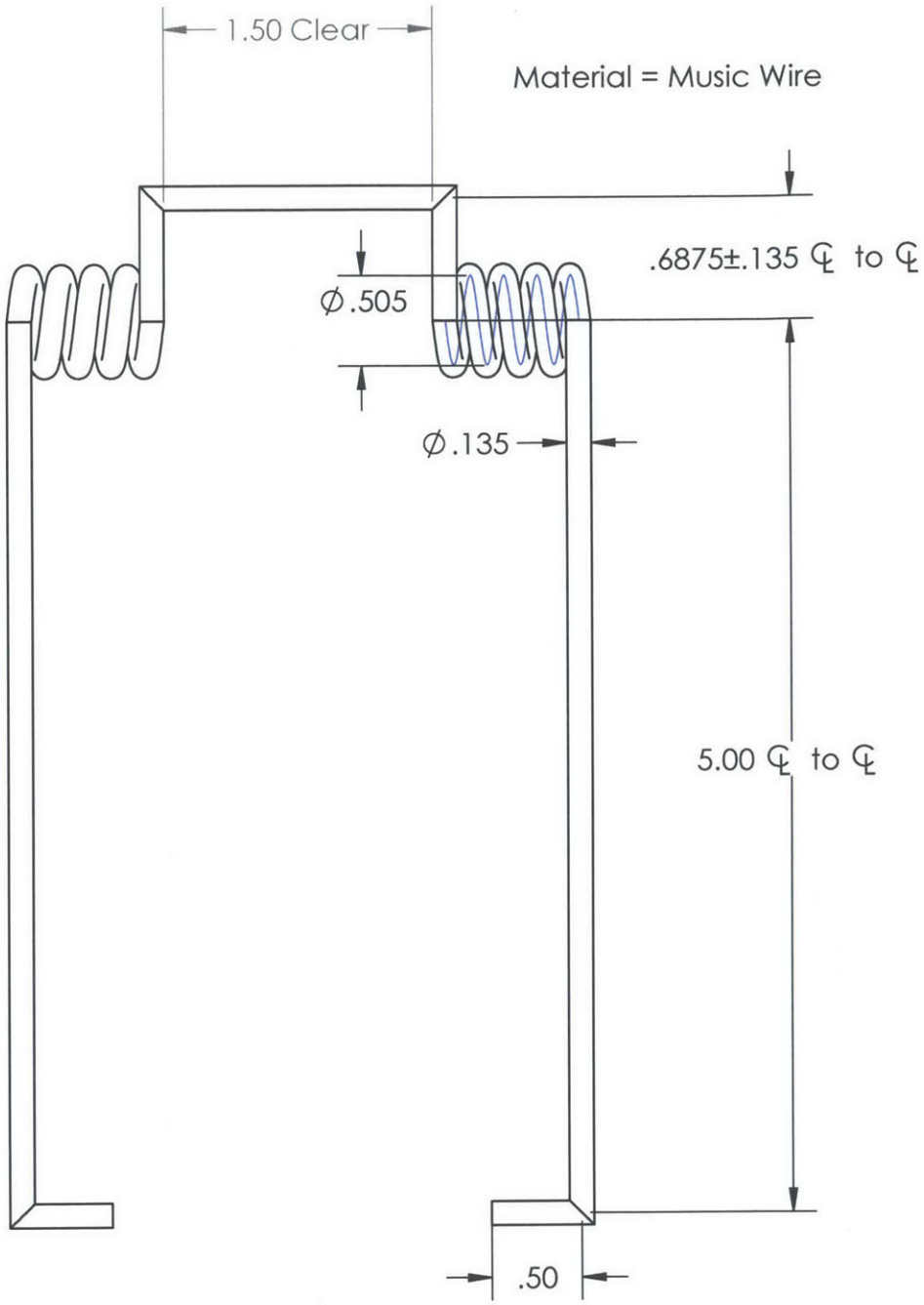

		DIMENSIONS ARE IN INCHES TOLERANCES: FRACTIONAL ± ANGULAR: MACH ± BEND ± TWO PLACE DECIMAL ± THREE PLACE DECIMAL ±		NAME	DATE
			DRAWN		
			CHECKED		
			ENG APPR.		
			MFG APPR.		
		MATERIAL	Q.A.		
NEXT ASSY	USED ON	FINISH	COMMENTS:		
APPLICATION		DO NOT SCALE DRAWING	SIZE A	DWG. NO. Torsional_Spring-Drawing	REV.
			SCALE:1:2	WEIGHT:	SHEET 1 OF 1

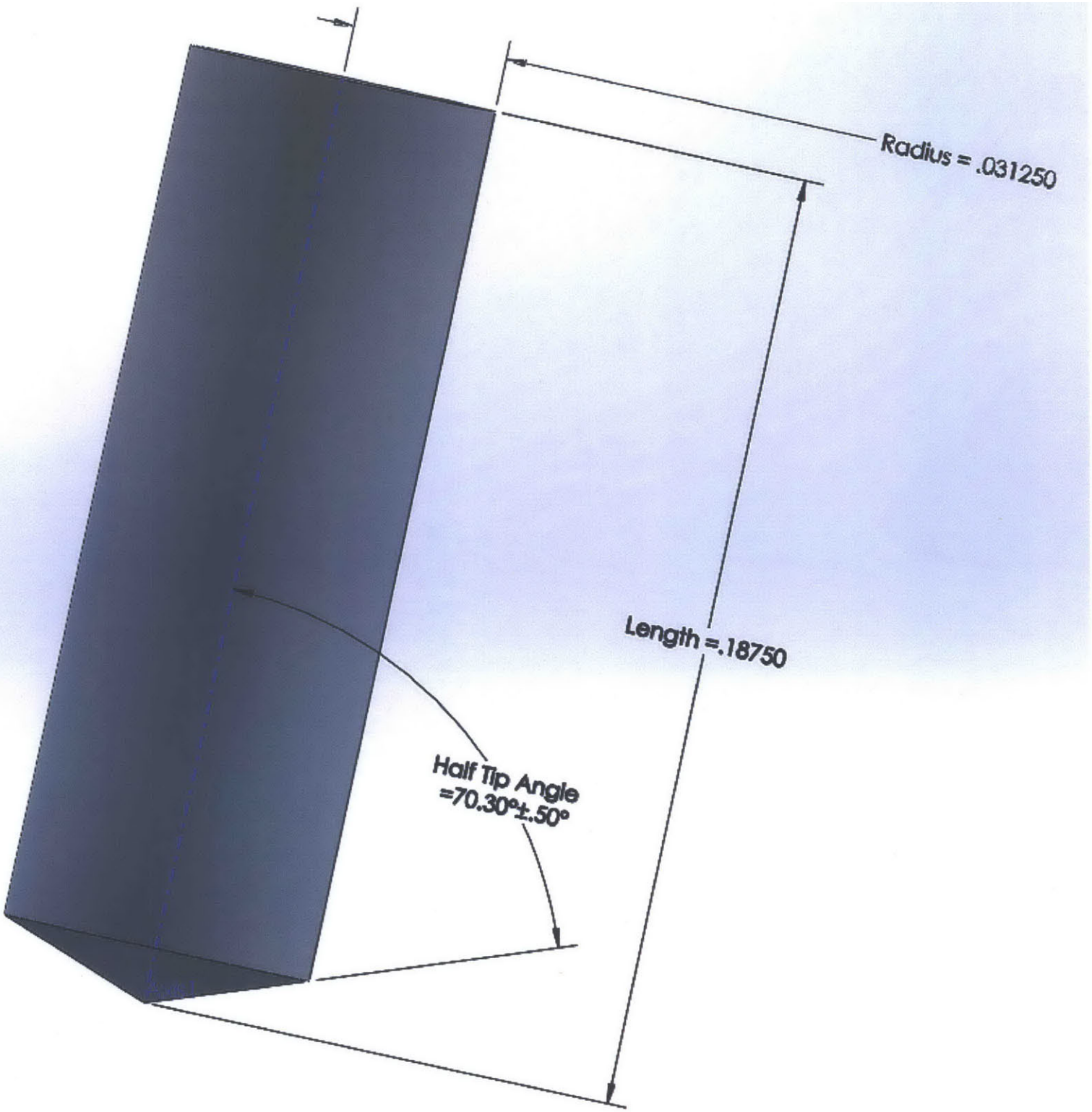
Radius = .031250
Length =.18750
Half Tip Angle
=70.30°±.50°